Influence of temperature and relative humidity on vapor hydration of an AVM nuclear waste glass

Sathya Narayanasamy, Patrick Jollivet, Loryelle Sessegolo, Frederic Angeli, Abdesselam Abdelouas

Influence of temperature and relative humidity on vapor hydration of an AVM nuclear waste glass

Sathya Narayanasamy[1*], Patrick Jollivet[1], Loryelle Sessegolo[2], Frederic Angeli[1*], Abdesselam Abdelouas[3]

[1] CEA, DEN, DES, ISEC, SEVT/LCLT, Marcoule, BP17171, 30207 Bagnols sur Cèze cedex, France

[2] LISA, UMR CNRS 7583, Université Paris-Est Créteil et Université Paris Diderot, Institut Pierre-Simon Laplace, 61, Avenue du Général de Gaulle, 94010 Créteil Cedex, France

[3] SUBATECH, CNRS-IN2P3, IMT Atlantique-Université de Nantes, 4 rue Alfred Kastler, BP 20722, 44307 Nantes cedex 03, France

Corresponding Authors: Frederic Angeli (frederic.angeli@cea.fr), Sathya Narayanasamy (sathyachem.kec@gmail.com)

Abstract

The safety assessment of the geological disposal of nuclear waste glasses requires a thorough understanding of the vapor hydration mechanisms of these glasses. In this context, the effect of temperature and relative humidity on vapor hydration of the AVM6 glass, which is the most reactive among the studied French AVM glasses, was investigated in the present study. Polished glass monoliths were vapor hydrated for 1 year (i) at 97% relative humidity (RH), at temperatures 70°C and 90°C to study the effect of temperature and (ii) at 50°C and 50% RH, 76% RH, 88% RH and 97% RH to study the effect of RH. The altered glass samples were characterized by SEM, XRD and ToF-SIMS. The results were compared with published results of AVM6 glass vapor hydrated at 50°C and 95% RH. The nature of the secondary phases that precipitate varied with both temperature and relative humidity, leading to variation in the behavior of elements in the altered layer (gel) but the altered layer morphology is similar at all temperatures studied. The Arrhenius law for temperature dependence is respected between the temperature range 50-90°C and the activation energy suggests that network-hydrolysis is the predominant rate controlling mechanism at these temperatures and duration. The secondary phases that incorporate transition metals and rare-earth elements are identified by XRD only in experiments conducted at lower RH values.

Keywords: Vapor hydration, glasses, gel layer, secondary phases, mechanisms

1. Introduction

Glass is generally considered to be a stable matrix that can remain chemically durable for hundreds of thousands of years, based on geological and archeological evidence [1], [2]. It can also be versatile in terms of composition, due to its capability to incorporate a wide variety of elements in its structure. Due to these properties, it is the chosen matrix for isolation and disposal of highly radioactive waste elements in a deep geological repository. Although considered chemically durable, depending on intrinsic glass properties and environmental conditions, glass gets corroded by water, whether in immersed conditions (aqueous medium) or exposed to humidity (vapor phase). According to the scenario projected for the deep geological waste disposal of nuclear waste glass packages in France [3], it is predicted that the nuclear waste glasses could be exposed to unsaturated medium for tens of thousands of years before subsequent aqueous alteration. Therefore, studies on the vapor phase hydration of the French nuclear waste glasses have been published fairly recently [4]–[9]. Vapor hydration of nuclear waste glasses was also a possibility in the scenario projected by the Yucca mountain project for the American nuclear waste disposal [10]. Therefore, many studies that focus on vapor hydration of American nuclear waste glasses have also been published [10], [11], [20], [12]–[19][21]. Vapor hydration studies have also been conducted on archeological or volcanic glasses with a goal to either study the phenomenon of Obsidian hydration dating [22]–[26] or to draw analogies between long-term vapor hydration of nuclear glasses and atmospheric corrosion of natural glasses [27]–[29]. Atmospheric alteration of medieval, historic glasses, stained-glass windows of Cathedrals and glass artefacts in museums have been studied in order to understand the phenomenon and preserve these glasses from further degradation [30]–[36]. These studies have helped to estimate vapor hydration rates for different glass compositions, identify glass alteration products and secondary phases. Basic glass-water reaction mechanisms such as molecular water diffusion, inter-diffusion with some loss of alkali/alkaline-earth elements and network hydrolysis have been identified through these studies. Nevertheless, a general trend of evolution of vapor hydration mechanisms over time has not yet been established. While some studies identify network-hydrolysis as the predominant vapor hydration mechanism for the studied duration [8], [33], certain alkali-rich glasses only show evidence of inter-diffusion reactions within the hydrated glass [36]. It has also been suggested that the predominant vapor hydration mechanism could change with increase in the duration of alteration from network-hydrolysis to diffusion of species through the gel layer formed [8]. Some studies have also shown an inflexion by a factor of 2 to 15 in vapor hydration rates in certain glass compositions [7], [8], [37]. The period around which this inflexion occurs is dependent on temperature, relative humidity and possibly glass

composition. An inflexion or acceleration of vapor hydration rate may also be triggered by the formation of secondary phases [16].

The effects of temperature and relative humidity on vapor hydration of glasses have been studied on different glass compositions [4], [7], [12], [15], [16], [23], [27], [37], [5], [17], [36]. In general, glass hydration rate increases both with temperature and relative humidity. Glass hydration rate may follow an Arrhenius law for temperature dependence and the diffusion rate of water can increase either linearly or exponentially with increasing relative humidity. Nevertheless, these studies have shown that glass response to these parameters can vary depending on the glass composition. It has also been established that vapor hydration mechanisms may not be the same at low (35-90°C) and high temperatures (90-200°C) [4], [7]. Apart from that, the activation energies vary across a wide range for different glass compositions and different studies. In short, the literature survey has shown the diversity and unpredictability associated with glass behavior in unsaturated medium and a unified model has not yet been established to predict vapor hydration rates at different environmental conditions. Adding to this, is the fact that the number of studies conducted on the vapor hydration of glasses is far lesser than the number of studies conducted on aqueous alteration of glasses. This highlights the necessity to extensively study vapor hydration of nuclear waste glasses to be able to carry-out the safety assessment of their geological disposal.

Therefore, this work was conducted within the framework of studying the behavior of the AVM (*Atelier de Vitrification de Marcoule*) nuclear waste glass behavior in unsaturated medium [8]. AVM glasses are complex borosilicate glasses made of more than 20 oxides and incorporate fission products from the UNGG (*Uranium Naturel Graphite-Gaz*) reactor at the Marcoule nuclear facility. For practical reasons, the glass studied here is an inactive simulant. The effects of temperature and relative humidity were investigated specifically on the AVM6 glass, since the previous study in this framework showed that among the different AVM glass compositions, AVM6 altered at the fastest rate in vapor phase at 50°C and 95% relative humidity [8].

2. Materials and methods

The composition of AVM6 glass in mole percent of oxides is provided in table 1. The synthesis of this glass has been described previously [38]. The glass samples used in this study and the cited study published earlier [8] were retrieved from the same batch.

2.1 Experiments

The section below describes the two sets of experiments that were performed, and the experiments are recapitulated in table 2. It is to be noted that in section 4, the results of the experiments described below are compared with the results of the study published earlier [8] since the glass samples were retrieved from the same batch and the experimental conditions are similar. However, the protocol used for glass alteration varies. This has also been addressed in section 4.

2.1.1 Effect of temperature

The AVM6 glass was altered in vapor phase at temperatures 70°C and 90°C and relative humidity 97% for a period of 1 year. The protocol used for glass alteration is based on literature [4]. Glass monoliths of dimensions 2.5x2.5x0.1 cm^3 were placed vertically in a Teflon walled stainless steel autoclave above 5.25 wt.% NaCl solution, which imposes a relative humidity of 97% [39]. The autoclave is placed inside an aluminum cylinder to prevent rapid heating and cooling cycles, which might induce water condensation on the glass monoliths. The setup is then put in an oven at 70°C or 90°C for a period of 1 year. At the end of the runs, the reactors were removed from the oven, allowed to cool down to ambient temperature and then the monoliths were stored in ambient conditions until characterization.

2.1.2 Effect of relative humidity

AVM6 glass monoliths of dimensions 2.5x2.5x0.1 cm^3 were altered in vapor phase at 50°C and four different relative humidity values (50±10%, 76±1%, 88±6% and 97±3%) for 1 year. The vapor hydration protocol used is different than the one used to study the effect of temperature and is described in detail in the reference [36]. It consists of an air-tight container equipped with a perforated shelf to hold samples and a tray below the shelf to contain the saturated salt solution, which will be used to impose the relative humidity in the container. This container was then placed in an oven at 50°C. At this temperature, saturated $MgNO_3$ solution was used to impose 50% RH, saturated NaCl solution was used to impose 76% RH, saturated KNO_3 solution was used to impose 88% RH and saturated K_2SO_4 solution was used to impose 97% RH. The relative humidity was measured using a sensor and the uncertainty in the relative humidity was measured from the standard deviation of the sensor measurements as well as taking into account 2% error associated with the sensor measurements. Due to some technical issues with the air-tight container, there was slight evaporation of the salt solution, which required frequent verification and adjustments. This resulted in fluctuations in the RH value, especially in the containers at 50% RH and 88% RH. At the end of one year of experiment, the samples were removed from the containers and placed in a desiccator (14% RH) until characterization.

2.2 Characterization techniques

SEM: Morphological analysis of the altered samples were carried out using a field emission Scanning Electron Microscope (SEM) Zeiss Gemini Supra 55, JEOL JSM 6330F with an Energy Dispersive Spectroscopy (EDS) system. The gel layer is identified visually through density differences between pristine glass and gel layer. The spatial resolution of the SEM does not permit to detect the presence of gel layers lower than 100 nm in thickness. EDS analysis can be used to identify secondary precipitates using compositional analysis, but the minimum specimen size required for EDS analysis is 1 to 2 µm (laterally and perpendicularly) to avoid signals from surrounding material. All samples were cut and observed directly (after metallization using carbon) by tilting the altered sample at an angle to observe the altered surface and eventually the presence of an altered layer at the cross-section. Additionally, all samples were enrobed in an epoxy resin, and polished to surface roughness < 1 µm to be observed in SEM for cross-section images.

XRD: The presence of crystalline secondary phases was analysed using a Philips X'Pert diffractometer X-Ray Diffraction (XRD) apparatus equipped with a copper tube ($\lambda_{K\alpha1}$=1.542 Å, voltage 40 kV and intensity 40 mA) and a goniometer (4-80° 2θ, step size 0.01744°). Each glass monolith was analyzed for 12 h on a multiple purpose sample stage (MPSS). The resulting peaks (if present) in the XRD pattern were treated with EVA software to identify the secondary phases corresponding to the peak [40].

ToF-SIMS: The behavior of elements in the altered layer was characterized using ToF-SIMS (SSIMS on TOF 5 (IONTOF)). Depth profiles of secondary positive ions were obtained by alternating analysis and abrasion cycles. 25 keV Bi_1^+ primary ions at 1.5 pA current were used for analysis cycles. 1 keV primary O_2^+ ions at 300 nA current were used for the abrasion cycles. The eroded area was 200x200 µm^2. The analyzed area was 50x50 µm^2. The surface charge was neutralized on the monoliths by a pulsed low-energy (<20 keV) electron flux. The depth calibration was carried out using the abrasion rate and a mechanical profilometer to measure the crater depth at the end of the analysis. It is to be noted that the same abrasion rate was used for analyzing the gel layer and the pristine glass. This choice was justified by the good correspondence between thickness of altered layer measured by SEM and ToF-SIMS in other works [7].

Thus at the end of the analysis, we obtain the intensities of different elements as a function of the depth of the sample analyzed (depth profiles). The profiles were normalized with respect to the intensity of each element (C) in the pristine glass (denoted as PG) and with respect to the intensity of Si (C_{Si}) at given depth as shown in the equation 2.2.1 below.

$$Normalized\ intensity = \frac{\frac{C}{C_{Si}}}{(\frac{C}{C_{Si}})_{PG}} \quad \text{Equation 2.2.1}$$

$$Altered\ layer\ depth = x_0\ at\ which \left(0.5 - \frac{\frac{C_B}{C_{Si}}}{\left(\frac{C_B}{C_{Si}}\right)_{PG}} = 0 \right) \quad \text{Equation 2.2.2}$$

In most of the vapor hydration studies, boron is the element that is the most depleted in the altered layer (in depth and in quantity), although it is surprising [4], [7], [8]. Retention of boron in the gel layer is often less than 10-20%. Therefore, it is used as a tracer to calculate the depth of the altered layer using equation 2.2.2. The depth of hydrogen penetration is compared to the thickness of boron depletion during vapor hydration. The hydrogen penetration depth is calculated from the ToF-SIMS profiles using equation 2.2.3 as shown below.

$$Depth\ of\ hydrogen\ penetration = x\ at\ which\ (H\ intensity = \frac{(\frac{\left(\frac{C_H}{C_{Si}}\right)}{(\frac{C_H}{C_{Si}})_{PG}})_{(gel\ layer)} + 1}{2}) \quad \text{Equation 2.2.3}$$

Many factors regarding the nature of the sample contribute to the uncertainties associated with the measurement of altered layer thickness by ToF-SIMS method. These factors are: (i) the surface roughness of the samples due to the presence of secondary precipitates, (ii) same speed of abrasion that was used to analyze the precipitates, gel and the pristine glass and (iii) the irregular and discontinuous alteration zones in case of heterogeneously altered samples. Since these factors were not quantifiable in this study, error values cannot be calculated. Nevertheless, ToF-SIMS analysis of different samples is useful to uniformly compare the samples, since 50 x 50 μm^2 is a relatively larger zone of analysis. It is also extremely useful to study the behavior of elements in the altered layer.

3. Results

3.1 Effect of temperature

SEM images

The SEM images of the AVM6 glass altered at 97% RH and at 70°C and 90°C (experiments 1 and 2 in table 2) are shown in figure 1. The surface of AVM6 glass altered at 70°C was covered with clusters/carpets of leafy secondary phases that were of an amoeboid shape. On the other hand, the surface of AVM6 glass altered at 90°C was covered entirely with a carpet of leafy secondary phases. The leafy precipitates on the surface of the sample altered at 90°C visually seems better developed than the

leafy precipitates on the surface of the sample altered at 70°C. The altered surface of both samples seemed to contain holes of a few hundred nm in size. The AVM6 glass altered at 90°C seemed to have more of these holes. The SEM image of the cross section of the AVM6 glass altered at 70°C shows a homogeneous gel layer of 290-350 nm thickness (figure 1(e) and figure S1 (e and f) in supplementary data). In the zone characterized by SEM, no holes were identified in the cross-sections. The SEM images of cross-sections of the AVM6 sample altered at 90°C shows the presence of several mushroom shaped holes that are a few µm deep and wide (also see figure S2 in supplementary data). Above these holes, the surface was covered with a gel layer of homogeneous thickness of about 1 µm.

XRD patterns

The XRD patterns of the AVM6 glasses altered at 70°C and 90°C are provided in figure S3 in supplementary data and the possible secondary phases identified through EVA software analysis of the peak patterns is summarized in the end in table 6. Although the protocol used for vapor hydration at 70°C and 90°C used NaCl to impose relative humidity, no peaks to indicate the presence of NaCl were identified. The sample altered at 90°C showed the presence of a small peak around 20° (2θ) (around 4.5 Å in d-scale) and 24.5° (2θ) (around 3.6 Å in d-scale) that indicates the presence of alumino silicates (possibly neosilicates or clay minerals). The AVM6 glass altered at 70°C did not show any peaks other than RuO_2 (platinoids that did not get incorporated in the network during glass preparation). However, the background subtracted XRD pattern seemed to contain peaks merged with the background noise around the same region (20° and 24.5° (2θ)) (see figure S4 in supplementary data).

ToF-SIMS profiles

The ToF-SIMS profiles of the AVM6 sample altered at 70°C and 90°C are provided in figures 2 and 3 respectively. The thicknesses of the altered layers measured by the depths of boron depletion (equation 2.2.2) are provided in table 3.

The ToF-SIMS profiles of the AVM6 glass vapor hydrated at 70°C show that (figure 2), apart from hydrogen penetration, formation of SiOH and boron depletion, the alkali and alkaline-earth elements are very mobile in the gel layer. It seems that these elements have migrated towards the surface of the gel layer probably to form secondary precipitates. From these profiles, it looks like the first 40-80 nm in the ToF-SIMS profiles are secondary precipitates. The migration of alkali and alkaline-earth elements has resulted in a depletion of these elements in the gel layer close to the gel-glass interface. The depletion of rare-earth elements and transition metals towards the surface of the altered sample could be due to the presence of a layer of precipitates close to the surface that does not incorporate these elements. (See

figure S5 in supplementary data for un-normalized ToF-SIMS profiles which also show this depletion). This could mean that there is no real loss of rare-earth elements and transition metals. The migration of alkali and alkaline-earth elements towards the surface could be either to form precipitates such as carbonates or to play a charge balancing role in the phyllosilicates that were seen in the SEM images (figure 1).

The ToF-SIMS profiles of all the elements in the gel layer of AVM6 glass altered at 90°C (figure 3) resemble that of the AVM6 glass altered at 70°C, except, the thickness of the altered layer is 1 µm and the thickness of the layer of secondary precipitates (based on the depth of depletion of rare-earth elements and transition metals, and the mobility of alkali and alkaline-earth elements) is around 250 nm.

3.2 Effect of relative humidity

SEM Images

Figure 4 shows the SEM images of the AVM6 samples vapor hydrated at 50°C and 97% RH and 88% RH for 1 year (experiments 6 and 5 respectively in table 2). On the surface of the AVM6 sample vapor hydrated at 97% RH, circular clusters of fibrous secondary precipitates of a few µm diameters are present along with fewer shapeless clusters of fibrous phases (also see figure S6(a) in supplementary data). The SEM image of the cross-section of the sample shows an altered layer of approximately 200 nm thickness, which could be most likely a layer of fibrous secondary precipitates. In the section of the sample analyzed, many irregularly altered zones could not be identified (in the cited reference [8], many irregularly altered zones were identified on the same AVM6 glass altered at 50°C and 95% RH in the climatic chamber for 6 months and 18 months).

The surface of the AVM6 sample vapor hydrated at 88% RH also seemed very similar to the sample vapor hydrated at 97%. This sample could also contain some irregularly altered zones as shown in figure 4(e).

Figure S7 in supplementary data shows the SEM images of the AVM6 samples vapor hydrated at 50°C and 76% RH and 50% RH for 1 year (experiments 4 and 3 respectively in table 2). Visually these surfaces are different from each other and also are different from the surfaces of the samples altered at the two higher RH values. The figures S7 (a) and (d) show the altered surfaces of AVM6 samples altered at 76% RH and 50% RH respectively at the same magnification. The shapes of the secondary phases

formed on these surfaces are visually different. The sample altered at 50% RH seems to contain more singular needle-like precipitates and there are circular spots on the altered surface that appear bulged. No such bulged zones are visible on the sample altered at 76% RH. However, the surface looks scaled, as though it could be a more advanced stage of the bulged zones that have peeled off. A few singular needle-like precipitates were visible on the sample altered at 76% RH as well.

XRD patterns

Figure S8 in supplementary data shows the XRD patterns of the AVM6 glass altered in all four RH values and the possible secondary phases identified through EVA software analysis of the peak patterns is summarized in the end in table 6. At all 4 RH values, a peak around 6° (2θ) (or 15 Å) is present indicating the formation of an aluminosilicate containing Na, Mg and Fe. The intensity of the peak increases with increasing relative humidity, suggesting that either a higher quantity of this phase had precipitated with increasing relative humidity or that as the relative humidity increases, the crystallinity of the precipitates improve. This peak was present on the same AVM6 samples altered at 50°C and 95% RH for 6 months and 18 months in the cited reference as well [8] and the composition of the phase was identified to be similar to that of montmorillonite, based on XRD and TEM analyses.

Only the AVM6 samples altered at lower RH values, 50% and 76% RH, contain peaks around 10° and 19.2° (2θ) (around 9.2 and 4.6 Å in d-scale), which could be $Nd_2(CrO_4)_3.7H_2O$ or $Pr_2(CrO_4)_3.7H_2O$ (see figure S9 in supplementary data). Usually, Nd gets incorporated in phases such as powellite ((Ca, Nd)MoO_4) or saponite (smectite clay mineral) [41], but these phases were not identified. These two samples also contain a peak at 15° (2θ) (around 6 Å in d-scale), which could hypothetically be attributed to sodium aluminosilicate hydrates and a peak at 32° (2θ) (around 2.8 Å in d-scale) which indicates the presence of NaCl. While the presence of NaCl on the AVM6 sample altered at 76% RH was expected since NaCl was used to impose relative humidity, its presence on the AVM6 sample altered at 50% RH is puzzling since $MgNO_3$ was the salt used to impose relative humidity. One of the possible explanations could be that the Cl was sourced from the tap water used to impose the relative humidity, although its concentration was much lower than in the NaCl salt solution

For the AVM6 samples altered at 88% and 97% RH, in addition to the peak at 6° (2θ), there are also peaks at 8°, 10°, 12° and 14° (2θ) (around 11, 8.8, 7.5 and 6.3 Å in d-scale) that correspond to sodium alumino silicates, possibly zeolites such as mordenite and stellerite (see supplementary data figure S10).

ToF-SIMS profiles

Table 4 provides the altered layer depths (boron depletion) and the depths of hydrogen penetration through the surface of the AVM6 glasses altered in all 4 RH values calculated using equation 2.2.2 and 2.2.3. Figure 5 presents the ToF-SIMS profiles of the AVM6 sample altered at 50% RH and 50°C for 1 year (experiment 3 in table 2). The thickness of boron depletion is around 27 nm in the gel layer, which is a little higher than the boron depletion in a pristine AVM6 glass (14 nm (figure S11 in supplementary data)). Transition metals and rare-earth elements are depleted in the first 10-20 nm of the altered layer, which was the case in pristine samples as well (figure S11 in supplementary data). The depletion of Ba, Sr and Li is slightly deeper than the depletion of boron in the AVM6 glass altered at 50% RH. The retention of boron in the first 20 nm of the altered layer is only between 2-10%. It seems as though the altered layer might be heterogeneous since the altered layer-glass interface of hydrogen penetration is larger than the thickness of altered layer and according to the profile of boron, its concentration is not uniform in the altered layer and the interface is also large. However, it cannot be ascertained because large interfaces may also be caused by the presence of secondary precipitates on the altered surface. The thickness of the layer is smaller than the resolution of SEM, so the assumed heterogeneity of the altered layer cannot be verified.

Figure 6 shows the ToF-SIMS profiles of the AVM6 glass altered at 76% RH (experiment 4 in table 2). The altered layer depth is 190 nm and the thickness of hydrogen penetration is 200 nm. Similar to the AVM6 glass altered at 50% RH, the retention of boron is around 2-10% in the altered layer. The retention of Na in the altered layer is uniform and is around 40%. The other alkali and alkaline-earth elements are depleted in the part of the altered layer that is close to the altered layer-glass interface and their concentration increases towards the surface of the altered glass. Such a profile suggests that the elements have migrated towards the surface probably to form secondary precipitates. Ba is the most mobile alkaline-earth element, with only 1-4% retention in the altered layer close to the interface. The retention factors of Ca, Sr and Li in this region are also only around 10%. The transition metals and the rare-earth elements are depleted in the first 20-40 nm of the altered layer. Contrary to the behavior of the other transition metals, the retention factor of Mn declines continually in the altered layer towards the altered surface until it is only 2-3% retained and Cr is enriched in the altered layer and depleted only towards the surface.

Figure 7 shows the normalized ToF-SIMS profiles of the elements for the AVM6 glass altered at 88% RH (experiment 5 in table 2). The altered layer thickness is around 124 nm and the thickness of

hydrogen penetration is around 129 nm. This thickness value is surprising since it is lower than the altered layer thickness of the AVM6 glass altered at 76% RH for the same temperature and duration. As seen from figure 4(e), the AVM6 glass altered at 88% RH has a heterogeneous altered layer. Therefore, the reason for this unexpectedly lower altered layer thickness could be that the ToF-SIMS analysis might have been done in a region with fewer irregularly altered zones or it could be associated with uncertainties in the measurement. Apart from this discrepancy, the behavior of elements in the altered layer is quite similar to that of the AVM6 glass altered at 76% RH in terms of shape of the profiles and the retention factors of elements in the altered layer (except Mn). The Mn behavior in this glass is quite similar to the behavior of other transition metals in the altered layer.

Figure 8 shows the normalized ToF-SIMS profiles of the AVM6 glass altered at 97% RH (experiment 6 in table 2). The altered layer thickness is around 540 nm and the thickness of hydrogen penetration is around 620 nm. Similar to the AVM6 glass altered at 50% RH, the altered layer-glass interface is quite large. It seems that the altered layer could be heterogeneous in this case as well, keeping in mind that the heterogeneity could also be caused by surface irregularities (presence of secondary precipitates). The rare-earth elements and the transition metals are immobile in the altered layer except the first 30-50 nm, where they seem to be slightly depleted probably due to the presence of secondary precipitates in this region. Once again, the alkali and the alkaline-earth elements are very mobile in the altered layer. They are depleted in the part of the altered layer close to the altered layer-glass interface and their concentration increases towards the surface. Na seems to be enriched in the first 250 nm of the altered layer (towards the surface).

4. Discussion

4.1 Effect of temperature

At the end of the experiment, the autoclaves in their aluminum over-container were removed from the oven and cooled to ambient temperatures before they were opened to retrieve samples. There is a risk that water may condense onto the samples during the cooling as a result of the reducing temperature and the attainment of dew point. Consequently, some modifications may be made to the altered surface such as dissolution of some alteration products and removal of some elements. However, we did not find any markers to indicate explicitly that water had condensed onto the sample surfaces. The ToF-SIMS profiles indicated the loss of boron from the altered layer. It was mentioned in the

previous study [8] that the loss of boron may be attributed to transportation in the vapor phase. The mobility of the alkaline-earth elements may be controlled by the precipitation of clay minerals.

Comparison of altered layer morphology: In a previous study, the altered layer morphology of the vapor hydrated AVM6 glass was already shown to be rather unusual [8]. It consisted of two types of alteration layers on the same glass samples vapor hydrated at 50°C and 95% RH for 181 days and 557 days. The altered surface contained a rather homogeneous continuous gel layer that was only a few tens of nm thick in addition to intermittently present, irregularly shaped and highly porous altered zones.

In this study, the SEM images described in section 3.1 show that a similar morphology has been observed on AVM6 samples vapor hydrated at 70°C and 90°C as well. The SEM images of the glass surface altered at 70°C showed the presence of what seems to be holes beneath the carpet of phyllosilicates (figure 1 (c)), although present rather infrequently in comparison with the sample altered at 90°C. As can be seen from figure S2(f) in supplementary data, these mushroom-shaped holes may not be completely empty, but may be of very low density based on the contrast in electronic density. Based on the SEM observations, figure 9 shows a schematic description of the possible altered layer morphology of AVM6 glass at different temperatures. The thickness of the homogeneous gel layer increases almost exponentially with temperature. Similarly, at 50°C, what seemed to be highly porous irregular zones might have developed into even more porous cup-shaped zones at 90°C, which seems to be a more advanced stage of corrosion. This type of corrosion seems to resemble sub-surface pitting corrosion commonly observed in steel or aluminum alloys due to slight inhomogeneity in the composition of the initial matrix [42]. Although the mushroom type shape of these cups is rather interesting because, dissimilarly, in pitting corrosion, usually oval holes with a pointy tip are observed. It was discussed in the earlier work [8] that it seems that the homogeneous gel layer and the irregular pitting type alteration are two separate processes occurring in parallel. The altered layer morphology is very similar at all the studied temperatures since a homogeneous gel layer in addition to intermittently present irregular altered zones are present in all three cases.

Calculation of activation energies: Next, the temperature dependence of vapor hydration rate on Arrhenius law is verified, as this might provide some insights into vapor hydration mechanisms. Glass alteration in aqueous medium is a thermally activated process. Several studies have shown that the dependence of the overall glass dissolution rate (k) on temperature follows Arrhenius law ($k = A_0 e^{\frac{-E_a}{RT}}$) [43], [44]. When the Arrhenius law is valid in a given temperature range, it means that glass alters by the

same mechanism in that range [43]. The term “overall glass dissolution rate” was used because all the reactions resulting in glass alteration such as water diffusion, ion-exchange and network hydrolysis are thermally activated. Therefore, it is difficult to identify the activation energy of individual reactions in the glass alteration process. Nevertheless, the experiments in the literature have permitted to estimate that an activation energy of around 65-75 KJ mol^{-1} suggests that glass alteration occurs mostly by network hydrolysis [44], [45]. An activation energy below 50 KJ mol^{-1} suggests that inter-diffusion is the predominant glass alteration mechanism [43]. It is usually considered that activation energies in-between these two ranges indicate glass alteration by both network hydrolysis and inter-diffusion mechanisms.

The vapor hydration of glasses is also a thermally activated process. Literature survey has shown that the dependence of vapor hydration rate (r_h) on temperature in a given range follows Arrhenius law only for certain glass compositions [36]. For example, in the study conducted on vapor hydration of alkali/alkaline-earth-silicate glasses in the temperatures 20°C and 50°C in one case [36] and 40°C and 80°C in another case [46], the vapor hydration rate did not follow Arrhenius law for temperature dependence. On the other hand, the vapor hydration rate of the SON68 glass follows Arrhenius law for temperature dependence in range 125-200°C with an activation energy of 43-47 KJ mol^{-1} [47] and an activation energy of 34±4 KJ mol^{-1} [7] in the temperature range 35-90°C. The difference in activation energy between these two temperature ranges is not very high. The activation energy value suggests that the mechanism which controls r_h is interdiffusion in both the temperature ranges for the studied duration, but at higher temperatures, the importance of hydrolysis with respect to interdiffusion increases. This is logical because, in general the activation energies are lower for interdiffusion reactions than hydrolysis reactions. Activation energies measured in other studies in various conditions vary from 34 KJ mol^{-1} to 137 KJ mol^{-1} [16], [24], [48], [49].

Calculation of activation energy between 70°C-90°C: For experiments 1 and 2 in table 2, we calculate the vapor hydration rate, first in m/day (by dividing the thickness of the homogeneous gel layers measured using SEM images (table 3) by the duration of alteration) and multiply it by the glass density to obtain the vapor hydration rate in g $m^{-2}day^{-1}$ (r_h, which is considered equivalent to k in the equation given above) after 1 year of alteration. While making this calculation, it is assumed that the vapor hydration rate has been constant for the duration of the experiment (1 year). This can be justified since at 50°C and 95% RH, it was shown in earlier work that the vapor hydration rate of the AVM6 glass is constant up to about 6 months approximately [8]. At 70°C and at 90°C, the vapor hydration rate must remain constant

for a longer duration since in literature it has been observed that at higher temperatures, the inflexion in vapor hydration rate takes longer to occur [7], [37]. In the cited literature, the vapor hydration kinetics was followed using FTIR spectroscopy for the SON68 glass; at 50°C, the vapor hydration rate was constant until 200 days, whereas at 90°C, the vapor hydration rate remained constant until almost 600 days [7]. Using the vapor hydration rates measured at only these two temperatures (70°C and 90°C) and the equation $\frac{d(\ln(V_H)}{dT} = \frac{E_a}{RT^2}$, we can calculate an activation energy of 62.3±12.5 KJ mol^{-1} (see table 5 for vapor hydration rates) for the AVM6 glass.

Calculation of activation energy between 50°C-90°C: We also have data on vapor hydration of AVM6 glass at 50°C and 97% RH, which can be included in the calculation of activation energies. However, the data obtained in the current study at 50°C (table 4, thickness of the altered layer formed at 50°C and 97% RH for 1 year (experiment 6) measured using ToF-SIMS) cannot be used because the experiment was conducted for 1 year and the previous study showed that the vapor hydration rate is definitely not constant up to 1 year of alteration [8]. Additionally, analysis by TEM is required to study the morphology of the altered layer and find out the presence and if so, the thickness of the homogeneous gel layer, which seems to be only a few tens of nm at 50°C [8]. The ToF-SIMS data cannot be used to measure the thickness of this homogeneous gel layer at 50°C This is due to the presence of the heterogeneous porous altered zones, which interfere with the ToF-SIMS analysis carried out on a relatively large section of the sample (50x50 µm^2), contrary to TEM images. Therefore, the data from TEM images obtained in the earlier study [8] on the same AVM6 glass altered at 50°C and 95% RH was used for the calculation of activation energy. In this cited reference [8], the vapor hydration kinetics was followed using FTIR spectroscopy. It showed that the vapor hydration rate was constant for the first 200 days approximately and then the rate dropped by a factor of 5 and remained constant at the lower rate until 557 days. The thickness of the homogeneous gel layer was around 50 nm after 181 days of vapor hydration, according to TEM images [8]. Using the linear regression of the evolution of hydration kinetics up to 557 days measured using FTIR spectroscopy [8], it was estimated that the thickness of the homogeneous gel layer after 1 year is around 60 nm. Therefore, if we consider an average vapor hydration rate for 1 whole year (0.46x10^{-3} g m^{-2}day given in table 5), the activation energy calculated using the slope of evolution of ln(r_h) vs 1/T (K^{-1}) from 50°C to 90°C is around 68.7±13.7 KJ mol^{-1} (brown line in figure 10). On the other hand, if we consider the vapor hydration rate until the first six months, up until which the vapor hydration rate was constant (0.77x10^{-3} g/m^{2}day), then the calculated activation energy is around 55.8±11.2 KJ mol^{-1} (blue line in figure 10).

418 The calculated r_h values at 50°C (an average value calculated taking into account the inflexion of
419 the rate), 70°C and 90°C are provided in table 5. These vapor hydration rates were calculated only for the
420 thickness of the homogeneous gel layer formed on the surface and does not include the irregular
421 heterogeneously altered porous zones or the mushroom shaped holes that are intermittently present.

422 Figure 10 shows the evolution of $\ln(r_h)$ vs $1/T$ (K^{-1}) from 50°C to 90°C. The dependence of the rate
423 of vapor hydration (only the formation of gel layer, without including the 'pit' type irregular altered
424 porous zones) of the AVM6 glass follows Arrhenius law for temperature dependence with an activation
425 energy that may vary between 55-68 KJ mol^{-1}. This activation energy value suggests that the rate of
426 formation of the gel layer must be controlled predominantly by network hydrolysis reactions for the
427 studied duration in the temperature range 50°C to 90°C.

428 *Comparison of secondary phases:* Despite the similarity in the vapor hydration of AVM6 glass between
429 50°C and 90°C in terms of altered layer morphology and mechanism of formation of the gel layer, the
430 secondary phases that have precipitated are different, as can be seen from table 6. In previous work [8],
431 it was noted that the glass altered at 50°C and 95% RH during 6 months and 18 months had an intense
432 peak around 6° (15 Å) that indicated the presence of a smectite (probably montmorillonite). The glasses
433 altered at 70°C and 90°C however did not have the same secondary phases precipitated on their
434 surfaces.

435 Based on the similarity in altered layer morphology and rate controlling gel-layer formation mechanism
436 and the difference in the precipitation of secondary phases at three different temperatures, the 'pitting'
437 type corrosion observed in AVM6 glass is most likely a property of the glass and not related to the
438 identity of the secondary phases that precipitate. Pristine AVM6 glass is slightly inhomogeneous due to
439 the presence of RuO_2 platinoids (figure S12 in supplementary data). However, as far as our analysis goes,
440 the local presence of platinoids could not be directly correlated to the presence of irregular porous
441 zones. Platinoids were also present in another simulated nuclear waste glass, but the vapor hydration of
442 this glass did not result in a similar irregular altered layer morphology as seen in AVM6 [37]. This too
443 supports the argument that the platinoids probably do not play a role in the rather particular altered
444 layer morphology of the AVM6 glass. Although the presence of these non-uniformly present altered
445 zones merit further analysis to link them to alteration conditions, glass property or composition, it could
446 not be carried out in the current study.

447

4.2 Effect of relative humidity

Evolution of altered layer thickness as a function of RH: As explained in the introduction, the choice of AVM6 glass for studying the effect of relative humidity at 50°C was based on the fact that this glass altered the fastest among the six glasses studied earlier [8]. However, at the time of launching the experiment, it was unknown that the AVM6 glass alters in a heterogeneous manner. SEM images of the samples altered at 88% RH and 97% RH seem to confirm the heterogeneous alteration of the AVM6 glass. However, TEM analysis was not carried out to verify if these altered samples had the same altered layer morphology described in figure 9. Despite the possible heterogeneity of the altered layer and the uncertainty associated with it, we use ToF-SIMS measurements to quantitatively study the effect of relative humidity on the AVM6 glass samples that were analyzed in a more or less uniform manner. These altered layer thicknesses and the thicknesses of hydrogen penetration into the sample include the secondary precipitates, gel layer and possibly irregularly altered zones. They are plotted as a function of the relative humidity in figure 11. From 50% RH to 97% RH, it can be seen that the altered layer thickness increases more or less exponentially, except the discrepant value at 88% RH.

In literature, some studies have found that glass alteration rate evolves exponentially with increasing relative humidity [16], [26], [36] and other studies have found that the evolution is linear [50], [51][26]. A few studies have noted a threshold RH value below which glass alteration is negligible and beyond which the alteration rate increases exponentially. This threshold value varies between 60% and 90%, depending on the study (glass composition, temperature) [16]. In our study too, there seems to be a threshold value around 50-60%, below which glass alteration seems negligible.

Table 4 gives the depth of hydrogen penetration in the AVM6 glass samples altered at different RH values. Considering this depth as a "diffusion thickness, e", a diffusion coefficient, D can be calculated using the equation $e = 2\sqrt{\frac{Dt}{\pi}}$ based on Fick's law. The diffusion coefficient (calculated in $m^2\ s^{-1}$) (given in table 4) also evolves exponentially with relative humidity (figure 11). A normalized diffusion rate called relative rate has been calculated in order to compare with literature [51]. The cited reference has regrouped a number of studies on the effect of relative humidity on vapor hydration of glasses (different glass compositions and temperature). While comparing our data with the cited literature, it is clear that the evolution of the diffusion rate in our study is very similar to the evolution of the diffusion rate of an SRL131 glass, which is a borosilicate nuclear waste glass, altered in vapor phase at 202°C [16]. This shows

the effect of composition on a glass's response to change in relative humidity. Glass composition can influence the quantity of water adsorbed on the glass surface. The release of alkali by initial ion exchange reactions decreases the vapor pressure of water adsorbed on the surface of the glass and promotes additional water vapor condensation [52]. The dependence of adsorbed water quantity on the alkali content was demonstrated in the work done on an Obsidian glass and SRL165 glass as well [53]. Other factors such as glass surface roughness may also influence the quantity of water adsorbed [54].

Comparison of secondary phases: The effect of relative humidity on secondary phase precipitation is also noticeable from our results (as can be noted from table 6 which summarizes the secondary phases precipitated in all 6 experiments). The samples altered at 88% and 97% RH have the same precipitates. The peaks in the XRD pattern of AVM6 sample altered at 97% RH are more intense than those for the sample altered at 88% RH. This is most likely related to the faster alteration of the sample at 97% RH, due to the higher availability of water molecules. Some of the peaks are only present on the patterns of the AVM6 samples altered at 50% RH and 76% RH. These peaks indicate the presence of NaCl and hydrated oxides of rare-earth and transition elements. These precipitates have been identified despite the relatively low alteration of the AVM6 samples altered at 50% RH.

Comparison of behavior of elements in the altered layer: The ToF-SIMS profiles have not only revealed increasing alteration rate with increasing humidity, but certain elements such as Na, Mg, Al, Zr and other transition metals and rare-earth elements also show increased retention factor in the altered layer with increasing relative humidity. In order to facilitate comparison of the mobility and the retention of elements in altered layers of different thicknesses, a "percent altered layer" was used for normalization. "Percent altered layer" is calculated as $\frac{x}{x_0} * 100$, where x is any given depth and x_0 is the altered layer depth calculated from equation 2.2.2. Figure 12 shows the normalized intensity of Na, Mg, Zr, Al, Mn, Ni, Fe, Nd and Ca as a function of the "percent altered layer" for all four RH values. These figures show a clear influence of the relative humidity on the retention of different elements in the altered layer. This effect is particularly marked for Na and Mg. At a low RH (50%), the first 40% of the altered layer retains only 10-20% of Na and Mg, whereas at 97% RH, Na is enriched in the altered layer and retention of Mg is 100%. The enrichment of Na and Mg towards the surface in the altered layer formed at 97% RH must be due to their incorporation in phyllosilicates formed at the surface, since it was seen from the XRD patterns that the intensity of the peak attributed to phyllosilicates increased with increasing RH. When it comes to the elements Zr and Al, they are almost 100% retained in most of the altered layer for all RH values except at 50% RH, where Zr is depleted up to 80% and Al is depleted up to 50% in the altered

layer near to the surface. Similarly, Nd is also significantly depleted only in the altered layer formed at 50% RH. It was earlier discussed that the depletion of transition metals and rare-earth elements in the sample altered at 50% RH was similar to the depletion of these elements in the pristine samples (the first 10-20 nm). In case of Fe and Mn, they are depleted up to 90% in the altered layers formed at both 50% RH and 76% RH, but almost fully retained in the altered layers formed at higher RH values. The behavior of Ca is inverse to the all the other elements discussed above. In the altered layer formed at 50% RH, Ca is almost 100% retained. In the altered layers formed at higher RH values, the retention of Ca is only around 10% near the altered layer-glass interface but the enrichment increases towards the surface. The normalized intensity is not 1 even at 100% of the altered layer, meaning that the depletion of Ca is more profound than that of boron.

The reason for the influence of RH on the mobility of elements within the altered layer could be related to the pH of the water film on the surface of glass exposed to relative humidity, since pH affects the solubility of elements. The lower the RH, the lower the quantity of water adsorbed on glass surface will be and consequently the pH may be higher. . Here, hypotheses for migration mechanisms of these elements have not been discussed. But one of the suggestions is that the migration of elements towards surface may be facilitated by water condensation in gel porosity. It has already been discussed in earlier work that it is very likely that water condenses in the pores of the altered layer formed in vapor phase as well [8].

Looking at the possibility of variations in pH with changing relative humidity, it seems plausible the rate-controlling mechanisms may also vary. However, at all four RH values, the $pH_{50°C}$ values will still be basic. Therefore, network-hydrolysis may still be the predominant rate-controlling mechanism at all four RH values.

Comparison of vapor hydration in different protocols

The AVM6 sample in this study that was altered at 50°C and 97% RH for 1 year (experiment 6) can be compared with the AVM6 samples that were altered at 50°C and 95% RH for 6 months and for 18 months which are described in the cited reference [8]. The AVM6 monolith samples were retrieved from the same batch for both the studies. The difference between the study described in this work and the study described in the reference is the alteration protocol (apart from the duration of alteration and the slight variation in relative humidity). In this work, the AVM6 sample was vapor hydrated using a protocol where the sample was placed in an air-tight container above a saturated K_2SO_4 solution to impose the relative humidity. In the reference, the AVM6 sample was vapor hydrated in a WEISS WK64L climatic chamber regulated at 50°C and 95% RH. Ideally, the glass alteration in both protocols must be similar

since the temperature and relative humidity are nearly the same. But, a few differences are noticeable among the AVM6 samples altered in the two different protocols.

One of the remarkable differences lies in the ToF-SIMS profiles. In the ToF-SIMS profiles of the two samples altered in the climatic chamber, a layer of phyllosilicates of 250-350 nm thickness is distinguishable from the ToF-SIMS profiles through the behavior of all the elements including transition metals and rare-earth elements in the AVM6 glass.

In case of the sample altered in this study, a phyllosilicate layer of around 200 nm can be distinguished from the ToF-SIMS profiles through the profiles of the elements H, Na, Mg, Li and other alkali and alkaline-earth elements. However, aluminum, transition metals and rare-earth elements do not seem to be mobile at all. This could mean that the Si/X (where X is Al, a transition metal or rare-earth element) ratio in the gel layer, phyllosilicate layer and the pristine glass is the same for the sample altered in this study. The interface between the altered-layer and pristine glass is also different between the two samples altered in the climatic chamber and the samples in this study. The thickness of the altered layer measured using the boron ToF-SIMS profile in the sample altered in the climatic chamber for 6 months is 1060 nm, whereas the thickness measured on the sample altered in this study for 1 year is 541 nm. It is to be kept in mind that in both cases, the altered layer could be heterogeneous with more irregularly altered zones in one case than the other, explaining this variation in the overall altered layer thickness. The other factor that could have played a role is the fluctuation in the RH experienced in this study. However, this shows the necessity of in-depth analysis of altered layer morphology in case of the vapor hydrated samples.

The XRD patterns of all samples altered in two different protocols show the same peak at 6° (2θ), indicating the presence of an aluminosilicate incorporating Na, Mg and Fe. But, the sample altered in this study had some additional peaks at 8°, 10°, 12° and 14° (2θ) indicating the presence of other aluminosilicates, which were absent in the sample altered for a longer duration in the climatic chamber.

The differences in the samples due the different vapor hydration protocols used are not drastic, but seem to have affected the nature of some of the secondary precipitates (and thus, the element behavior in the altered layer) and the overall thickness of the altered layer.

5. Conclusion

The effect of temperature between 70°C and 90°C at 97% RH and relative humidity between 50% RH and 97% RH at 50°C on the vapor hydration of the AVM6 glass was studied. It was revealed that the altered layer morphology was similar at all temperatures (continuous gel layer of homogeneous thickness along with intermittently present irregularly altered zones). However, the nature/identity of the secondary phases and the behavior of the elements in the gel layer varied with temperature. Therefore, it is likely that the rather particular altered layer morphology of the AVM6 glass is dependent on the glass properties (could be inhomogeneity in glass composition) and not the nature of the secondary phases. The rate of formation of the homogeneous gel layer seems to follow Arrhenius law for temperature dependence in the ranges 50°C to 90°C. The value of the activation energy suggested that network hydrolysis was the predominant rate-controlling mechanism in the studied range for the studied duration, likely due to high pH values of the water film. Similar to the temperature effect, changing relative humidity too resulted in differences in some of the precipitated secondary phases and the nature of the altered layer. XRD patterns suggest that secondary phases incorporating rare-earth elements and transition metals (which are inactive simulants for radioactive actinides and fission products in nuclear waste) precipitate at the sample surface only at low RH experiments. Their mobility in the gel layer was also revealed to be high only at low RH experiments. This is rather a positive information from the point of view of geological disposal scenario since the RH values expected in the repository are close to saturation.

The results presented in this study show a few perspectives for future research. It is important from the point of view of safety assessment of geological waste disposal to carry-out in-depth characterization and stability/solubility studies of the radionuclide incorporating secondary phases that may form under expected repository conditions. Since it seems that pH may play a crucial role in determining the mobility of different elements in the altered layer, development of surface pH measurement protocols using advanced techniques need to be envisaged. It would also be useful in developing geochemical models to predict vapor hydration rates of different glass compositions. Vapor hydration experiments as a function of time need to be carried out to verify that vapor hydration rate is constant for the calculation of activation energy. Finally, the importance of comprehensive morphological analysis of vapor hydrated glass surfaces needs to be emphasized.

Acknowledgements

We would like to thank Jean-Pierre Mestre (CEA) and Marie Fenart (CEA) for the SEM images, Myriam Chartier (CEA) for XRD patterns, Laurent Dupuy and Elodie Chauvet (TESCAN Analytics) for the ToF-SIMS profiles. This study was supported by CEA and EDF (Electricité de France). We would like to particularly thank Florent Tocino and Hélène Schneider (EDF) for their support.

Data Availability

The SEM data supporting the findings are available within the article and the supplementary information. The processed data of ToF-SIMS and XRD are also available within the article and supplementary information. The raw data of the ToF-SIMS and XRD can be shared by the corresponding author upon reasonable request.

References

[1] I. Friedman and W. Long, “Volcanic glasses, their origins and alteration processes,” *J. Non. Cryst. Solids*, vol. 67, no. 1, pp. 127–133, 1984, doi: https://doi.org/10.1016/0022-3093(84)90144-3.

[2] A. Verney-Carron, S. Gin, and G. Libourel, “A Fractured Roman Glass Block Altered for 1800 years in Seawater: Analogy with Nuclear Waste Glass in a Deep Geological Repository,” *Geochim. Cosmochim. Acta*, vol. 72, pp. 5372–5385, Nov. 2008, doi: 10.1016/j.gca.2008.08.018.

[3] ANDRA-Collectif, “Dossier d’options de sûreté - Partie après fermeture (DOS-AF),” 2016.

[4] J. Neeway *et al.*, “Vapor hydration of SON68 glass from 90 °C to 200 °C: A kinetic study and corrosion products investigation,” *J. Non. Cryst. Solids*, vol. 358, no. 21, pp. 2894–2905, Oct. 2012, doi: 10.1016/J.JNONCRYSOL.2012.07.020.

[5] A. Abdelouas *et al.*, “A Preliminary Investigation of the ISG Glass Vapor Hydration,” *Int. J. Appl. Glas. Sci.*, vol. 4, pp. 307–316, Dec. 2013, doi: 10.1111/ijag.12055.

[6] A. A. Chaou, A. Abdelouas, Y. El Mendili, R. Bouakkaz, and C. Martin, “The French SON68 Glass Vapor Hydration under Different Atmospheres,” *Procedia Mater. Sci.*, vol. 7, pp. 179–185, Jan. 2014, doi: 10.1016/J.MSPRO.2014.10.024.

[7] R. Bouakkaz, A. Abdelouas, and B. Grambow, “Kinetic study and structural evolution of SON68 nuclear waste glass altered from 35 to 125 °C under unsaturated H2O and D2O18 vapour conditions,” *Corros. Sci.*, vol. 134, pp. 1–16, Apr. 2018, doi: 10.1016/J.CORSCI.2017.12.035.

[8] S. Narayanasamy *et al.*, “Influence of composition of nuclear waste glasses on vapor phase hydration,” *J. Nucl. Mater.*, vol. 525, 2019, doi: 10.1016/j.jnucmat.2019.07.015.

[9] A. Ait Chaou, A. Abdelouas, Y. El Mendili, and C. Martin, “The role of pH in the vapor hydration at 175 °C of the French SON68 glass,” *Appl. Geochemistry*, vol. 76, pp. 22–35, 2017, doi: https://doi.org/10.1016/j.apgeochem.2016.11.006.

[10] J. K. Bates, M. G. Seitz, and M. J. Steindler, “The relevance of vapor phase hydration aging to nuclear waste isolation,” *Nucl. Chem. Waste Manag.*, vol. 5, no. 1, pp. 63–73, Jan. 1984, doi: 10.1016/0191-815X(84)90008-1.

[11] J. K. Bates, W. L. Ebert, X. Feng, and W. L. Bourcier, “Issues affecting the prediction of glass reactivity in an unsaturated environment,” *J. Nucl. Mater.*, vol. 190, pp. 198–227, Aug. 1992, doi: 10.1016/0022-3115(92)90087-2.

[12] J. K. BATES, L. J. JARDINE, and M. J. STEINDLER, “Hydration Aging of Nuclear Waste Glass,” *Science (80-.).*, vol. 218, no. 4567, pp. 51 LP – 54, Oct. 1982, doi: 10.1126/science.218.4567.51.

[13] J. K. Bates, M. J. Steindler, and P. L. McDaniel, “Hydration of stressed nuclear waste glass,” *Mater. Lett.*, vol. 2, no. 4, pp. 296–300, Mar. 1984, doi: 10.1016/0167-577X(84)90136-8.

[14] J. K. Bates, M. J. Steindler, B. Tani, and F. J. Purcell, “The hydration alteration of a commercial nuclear waste glass,” *Chem. Geol.*, vol. 51, no. 1–2, pp. 79–87, Oct. 1985, doi: 10.1016/0009-2541(85)90088-9.

[15] T. A. Abrajano, J. K. Bates, and C. D. Byers, “Aqueous corrosion of natural and nuclear waste

glasses I. Comparative rates of hydration in liquid and vapor environments at elevated temperatures," *J. Non. Cryst. Solids*, vol. 84, no. 1–3, pp. 251–257, Jul. 1986, doi: 10.1016/0022-3093(86)90783-0.

[16] T. A. Abrajano, J. K. Bates, and J. J. Mazer, "Aqueous corrosion of natural and nuclear waste glasses II. Mechanisms of vapor hydration of nuclear waste glasses," *J. Non. Cryst. Solids*, vol. 108, no. 3, pp. 269–288, Apr. 1989, doi: 10.1016/0022-3093(89)90297-4.

[17] B. M. Biwer, J. K. Bates, T. A. J. Abrajano, and J. P. Bradley, "Comparison of the Layer Structure of Vapor Phase and Leached SRL Glass by Use of AEM." MRS Proceedings,176, 225, 1989, doi: 10.1557/PROC-176-255.

[18] J. K. Bates, T. J. Gerding, and A. B. Woodland, "Parametric effects of glass reaction under unsaturated conditions." MRS Proceeding, 176, 347, United States, 1989, doi: 10.1557/PROC-176-347.

[19] W. L. Ebert and J. K. Bates, "The reaction of synthetic nuclear waste glass in steam and hydrothermal solution," United States, 1989. doi: 10.2172/137671.

[20] W. L. Ebert, J. K. Bates, and W. L. Bourcier, "The hydration of borosilicate waste glass in liquid water and steam at 200 °C," *Waste Manag.*, vol. 11, no. 4, pp. 205–221, Jan. 1991, doi: 10.1016/0956-053X(91)90068-G.

[21] W. . Gong, L. . Wang, R. . Ewing, E. Vernaz, J. . Bates, and W. . Ebert, "Analytical electron microscopy study of surface layers formed on the French SON68 nuclear waste glass during vapor hydration at 200°C," *J. Nucl. Mater.*, vol. 254, no. 2–3, pp. 249–265, Apr. 1998, doi: 10.1016/S0022-3115(97)00349-8.

[22] I. Friedman and W. Long, "Hydration Rate of Obsidian," *Science (80-.).*, vol. 191, no. 4225, pp. 347 LP – 352, Jan. 1976, doi: 10.1126/science.191.4225.347.

[23] K. L. Hull, "Reasserting the Utility of Obsidian Hydration Dating: A Temperature-Dependent Empirical Approach to Practical Temporal Resolution with Archaeological Obsidians," *J. Archaeol. Sci.*, vol. 28, no. 10, pp. 1025–1040, Oct. 2001, doi: 10.1006/JASC.2000.0629.

[24] L. M. Anovitz, D. R. Cole, and M. Fayek, "Mechanisms of rhyolitic glass hydration below the glass transition," *Am. Mineral.*, vol. 93, no. 7, pp. 1166–1178, Jul. 2008, doi: 10.2138/am.2008.2516.

[25] L. M. Anovitz, D. R. Cole, and L. R. Riciputi, "Low-temperature isotopic exchange in obsidian: Implications for diffusive mechanisms," *Geochim. Cosmochim. Acta*, vol. 73, no. 13, pp. 3795–3806, Jul. 2009, doi: 10.1016/J.GCA.2009.02.035.

[26] J. J. Mazer, C. M. Stevenson, W. L. Ebert, and J. K. Bates, "The Experimental Hydration of Obsidian as a Function of Relative Humidity and Temperature," *Am. Antiq.*, vol. 56, no. 3, pp. 504–513, Mar. 1991, doi: 10.2307/280898.

[27] J. J. Mazer, J. K. Bates, C. R. Bradley, and C. M. Stevenson, "Water diffusion in tektites: An example of the use of natural analogues in evaluating the long-term reaction of glass with water," *J. Nucl. Mater.*, vol. 190, pp. 277–284, Aug. 1992, doi: 10.1016/0022-3115(92)90091-X.

[28] J. S. Luo, W. L. Ebert, J. J. Mazer, and J. K. Bates, "Simulation of natural corrosion by vapor hydration test: seven-year results." 1996, Accessed: Mar. 19, 2020. [Online]. Available: https://inis.iaea.org/search/search.aspx?orig_q=RN:28069027.

690 [29] T. A. J. Abrajano, W. L. Ebert, and J. S. Luo, “Natural analogues of nuclear waste glass
691 corrosion,” United States. [Online]. Available:
692 http://inis.iaea.org/search/search.aspx?orig_q=RN:32064831.

693 [30] J. Sterpenich and G. Libourel, “Using stained glass windows to understand the durability of
694 toxic waste matrices,” *Chem. Geol.*, vol. 174, no. 1–3, pp. 181–193, Apr. 2001, doi:
695 10.1016/S0009-2541(00)00315-6.

696 [31] T. Lombardo *et al.*, “Characterisation of complex alteration layers in medieval glasses,” *Corros.
697 Sci.*, vol. 72, pp. 10–19, Jul. 2013, doi: 10.1016/J.CORSCI.2013.02.004.

698 [32] L. Sessegolo *et al.*, “Long-term weathering rate of stained-glass windows using H and O
699 isotopes,” *npj Mater. Degrad.*, vol. 2, no. 1, p. 17, 2018, doi: 10.1038/s41529-018-0038-1.

700 [33] F. Alloteau *et al.*, “New insight into atmospheric alteration of alkali-lime silicate glasses,”
701 *Corros. Sci.*, vol. 122, pp. 12–25, Jul. 2017, doi: 10.1016/J.CORSCI.2017.03.025.

702 [34] P. Bellendorf, H. Roemich, S. Gerlach, P. Mottner, E. López, and K. Wittstadt, “Archaeological
703 glass: The surface and beyond,” *Glas. Ceram. Conserv. 2010 Interim Meet. ICOM-CC Work. Gr.*,
704 pp. 137–144, Jan. 2010.

705 [35] N. Papadopoulos and C. D. A., “Influence of weather conditions on glass properties,” *J. Univ.
706 Chem. Technol. Metall.*, vol. 4, no. 47, pp. 429–439, 2012.

707 [36] L. Sessegolo, “Utilisation de traceurs isotopiques pour l’étude des mécanismes et des
708 cinétiques d’altération des verres de vitraux en milieu atmosphérique,” PhD thesis of
709 Université Paris-Est Créteil Val-de-Marne, 2018.

710 [37] A. Ait Chaou *et al.*, “Vapor hydration of a simulated borosilicate nuclear waste glass in
711 unsaturated conditions at 50 °C and 90 °C,” *RSC Adv.*, vol. 5, no. 79, pp. 64538–64549, 2015,
712 doi: 10.1039/C5RA12384D.

713 [38] B. M. J. Thien, N. Godon, A. Ballestero, S. Gin, and A. Ayral, “The dual effect of Mg on the long-
714 term alteration rate of AVM nuclear waste glasses,” *J. Nucl. Mater.*, vol. 427, no. 1–3, pp. 297–
715 310, Aug. 2012, doi: 10.1016/J.JNUCMAT.2012.05.025.

716 [39] K. Pitzer, P. Rogers, and J. Peiper, “Thermodynamics of High Temperature Brines,” *Lawrence
717 Berkeley Lab. Nucl. Waste Isol. Geophys. Reserv. Eng., Geosci.*, pp. 152–154, Sep. 1982.

718 [40] “EVA software for phase analysis.” https://www.bruker.com/products/x-ray-diffraction-and-
719 elemental-analysis/x-ray-diffraction/xrd-software/eva.html.

720 [41] A. Abdelouas, J.-L. Crovisier, W. Lutze, B. Grambow, J.-C. Dran, and R. Müller, “Surface layers
721 on a borosilicate nuclear waste glass corroded in MgCl2 solution,” *J. Nucl. Mater.*, vol. 240, no.
722 2, pp. 100–111, 1997, doi: https://doi.org/10.1016/S0022-3115(96)00672-1.

723 [42] Y. Zhu *et al.*, “Metal pitting corrosion characterized by scanning acoustic microscopy and
724 binary image processing,” *Corros. Sci.*, p. 108685, Apr. 2020, doi:
725 10.1016/J.CORSCI.2020.108685.

726 [43] J. J. Mazer, “Temperature effects on waste glass performance,” United States, 1991. doi:
727 10.2172/5749349.

728 [44] J. D. Vienna, J. J. Neeway, J. V Ryan, and S. N. Kerisit, “Impacts of glass composition, pH, and
729 temperature on glass forward dissolution rate,” *npj Mater. Degrad.*, vol. 2, no. 1, p. 22, 2018,

730 doi: 10.1038/s41529-018-0042-5.

731 [45] P. Jollivet, S. Gin, and S. Schumacher, “Forward dissolution rate of silicate glasses of nuclear
732 interest in clay-equilibrated groundwater,” *Chem. Geol.*, vol. 330–331, pp. 207–217, Nov.
733 2012, doi: 10.1016/J.CHEMGEO.2012.09.012.

734 [46] F. Alloteau, “Contribution à la compréhension des mécanismes de l’altération atmosphérique
735 des verres et étude d’un traitement de protection à base de sels de zinc,” 2017.

736 [47] J. J. Neeway, “The alteration of the SON68 reference waste glass in silica saturated conditions
737 and in the presence of water vapor,” PhD thesis of University of Nantes, 2011.

738 [48] Y. Kudriavtsev, M. Avendano, G. Ramirez, R. Asomoza-Palacio, and L. Manzanilla-Naim,
739 “Water vapor interaction with borosilicate glass,” *Solid State Ionics*, vol. 321, pp. 122–125,
740 Aug. 2018, doi: 10.1016/J.SSI.2018.04.015.

741 [49] Y. Kudriavtsev, R. Asomoza-Palacio, and L. Manzanilla-Naim, “Interaction of water vapor with
742 silicate glass surfaces: Mass-spectrometric investigations,” *Tech. Phys. Lett.*, vol. 43, no. 5, pp.
743 447–449, 2017, doi: 10.1134/S1063785017050054.

744 [50] K. Cummings, W. A. Lanford, and M. Feldmann, “Weathering of glass in moist and polluted
745 air,” *Nucl. Instruments Methods Phys. Res. Sect. B Beam Interact. with Mater. Atoms*, vol.
746 136–138, pp. 858–862, 1998, doi: https://doi.org/10.1016/S0168-583X(97)00758-1.

747 [51] L. M. Anovitz, L. R. Riciputi, D. R. Cole, M. S. Gruszkiewicz, and J. Michael Elam, “The effect of
748 changes in relative humidity on the hydration rate of Pachuca obsidian,” *J. Non. Cryst. Solids*,
749 vol. 352, no. 52, pp. 5652–5662, 2006, doi: https://doi.org/10.1016/j.jnoncrysol.2006.08.044.

750 [52] J. C. Cunnane *et al.*, “High-Level Nuclear-Waste Borosilicate Glass: A Compendium of
751 Characteristics,” *MRS Proc.*, vol. 294, p. 225, 1992, doi: DOI: 10.1557/PROC-294-225.

752 [53] W. L. Ebert, R. F. Hoburg, and K. Bates, “The Sorption of Water on Obsidian and a Nuclear
753 Waste Glass,” *Phys. Chem. Glas.*, vol. 32, pp. 133–137, Aug. 1991.

754 [54] A. Jiřička, J. D. Vienna, P. Hrma, and D. M. Strachan, “The effect of experimental conditions
755 and evaluation techniques on the alteration of low activity glasses by vapor hydration,” *J.*
756 *Non. Cryst. Solids*, vol. 292, no. 1, pp. 25–43, 2001, doi: https://doi.org/10.1016/S0022-
757 3093(01)00875-4.

Tables

Table 1

Table 1 Composition of AVM6 glass in mol% oxides

Oxides	mol%	Oxides	mol%	Oxides	mol%
SiO_2	49.29	NiO	0.27	TeO_2	0.01
Al_2O_3	5.88	Cr_2O_3	0.20	Cs_2O	0.03
B_2O_3	18.64	P_2O_5	0.00	BaO	0.03
Na_2O	16.65	SrO	0.03	La_2O_3	0.02
CaO	0.24	Y_2O_3	0.01	Ce_2O_3	0.02
MgO	6.28	MoO_3	0.13	Pr_2O_3	0.01
Li_2O	0.89	MnO	0.05	Nd_2O_3	0.04
ZrO_2	0.10	Ag_2O	0.01	RuO_2	0.08
Fe_2O_3	0.79	CdO	0.26	PdO	0.05

Table 2

Table 2 Summary of experiments that were performed

Experiment No	Parameter studied	Temperature, °C	Relative humidity, %
1	Effect of Temperature	70	97
2		90	97
3	Effect of relative humidity	50	50±10
4		50	76±1
5		50	88±6
6		50	97±3

Table 3

Table 3 Thickness of the gel layer formed during vapor hydration of AVM6 glass at 70°C and 90°C at 97% RH for 1 year; (The ToF-SIMS thicknesses are based on the depth of boron depletion calculated from equation 2.2.2)

Experiment No		Thickness (SEM), nm	Thickness (ToF-SIMS), nm
1	**AVM6- 70°C**	300	390
2	**AVM6- 90°C**	1000	1050

Table 4

Table 4 Thickness of the diffusion of hydrogen into the surface of the altered glass, thickness of boron depletion (gel layer thickness) and the diffusion coefficient calculated from the thickness of hydrogen diffusion for the AVM6 glass altered in vapor phase at 50°C and x% relative humidity for 1 year . The given values are measured from ToF-SIMS profiles normalized with respect to pristine glass and Si intensity. The uncertainties associated cannot be calculated as explained in section 2.2

Experiment No	Relative humidity, %	Thickness (hydrogen), nm	Thickness (boron), nm	Diffusion coefficient, m^2/s
3	**50**	31	27	2.39×10^{-23}
4	**76**	200	190	9.96×10^{-22}
5	**88**	129	124	4.14×10^{-22}
6	**97**	620	541	9.57×10^{-21}

Table 5

Table 5 Calculated vapor hydration rates (r_h) used to study if the temperature dependence of the vapor hydration rates follows Arrhenius law; The experiments were carried out for 1 year at 97%RH (for 70°C and 90°C) and 95%RH (for 50°C); (* calculated value)

Experiment No	Temperature, °C	Thickness of homogeneous gel layer after 1 year of vapor hydration, nm	Vapor hydration rate, g m^{-2}day ($x10^{-3}$)
Data from literature [8]	**50**	60*	0.46
1	**70**	300	2.3
2	**90**	1000	7.67

Table 6

Table 6 Summary of secondary phases precipitated in all the six experiments based on the analysis by EVA software of the peaks in the XRD pattern

Experiment No	Peaks in XRD pattern (2theta)	Secondary phases
1	20°, 24.5° (?)	Alumino silicates/neosilicates/clay minerals (Chloritoid? Tosudite ?)
2	20°, 24.5°	Alumino silicates/neosilicates/clay minerals (Chloritoid? Tosudite ?)
3	6°	Aluminosilicate containing Na, Mg, Fe (Vermiculite? Montmorillonite?)
	10°, 19.2°	$(Nd_2(CrO_4)_3.7H_2O$? or $Pr_2(CrO_4)_3.7H_2O$?)
	15°	Sodium aluminosilicate hydrates?
	32°	NaCl
4	6°	Aluminosilicate containing Na, Mg, Fe (Vermiculite? Montmorillonite?)
	10°, 19.2°	$(Nd_2(CrO_4)_3.7H_2O$? or $Pr_2(CrO_4)_3.7H_2O$?)
	15°	Sodium aluminosilicate hydrates?
	32°	NaCl
5	6°	Aluminosilicate containing Na, Mg, Fe (Vermiculite? Montmorillonite?)
	8°, 10°, 12°, 14°	Sodium aluminosilicates / zeolites (Mordenite? Stellerite?)
6	6°	Aluminosilicate containing Na, Mg, Fe (Vermiculite? Montmorillonite?)
	8°, 10°, 12°, 14°	Sodium aluminosilicates / zeolites (Mordenite? Stellerite?)

Note for table 6: All AVM6 glasses contain peaks at approximately 28°, 35°,40° and 54° due to the presence of platinoids (RuO_2) in the pristine glass. The secondary phases have been identified by analysis of XRD patterns using EVA software. The question marks have been added to indicate that these are possibilities and a more thorough analysis would be required to confirm their presence. (?)The peaks seem to be present after background subtraction.

Figures

Figure 1

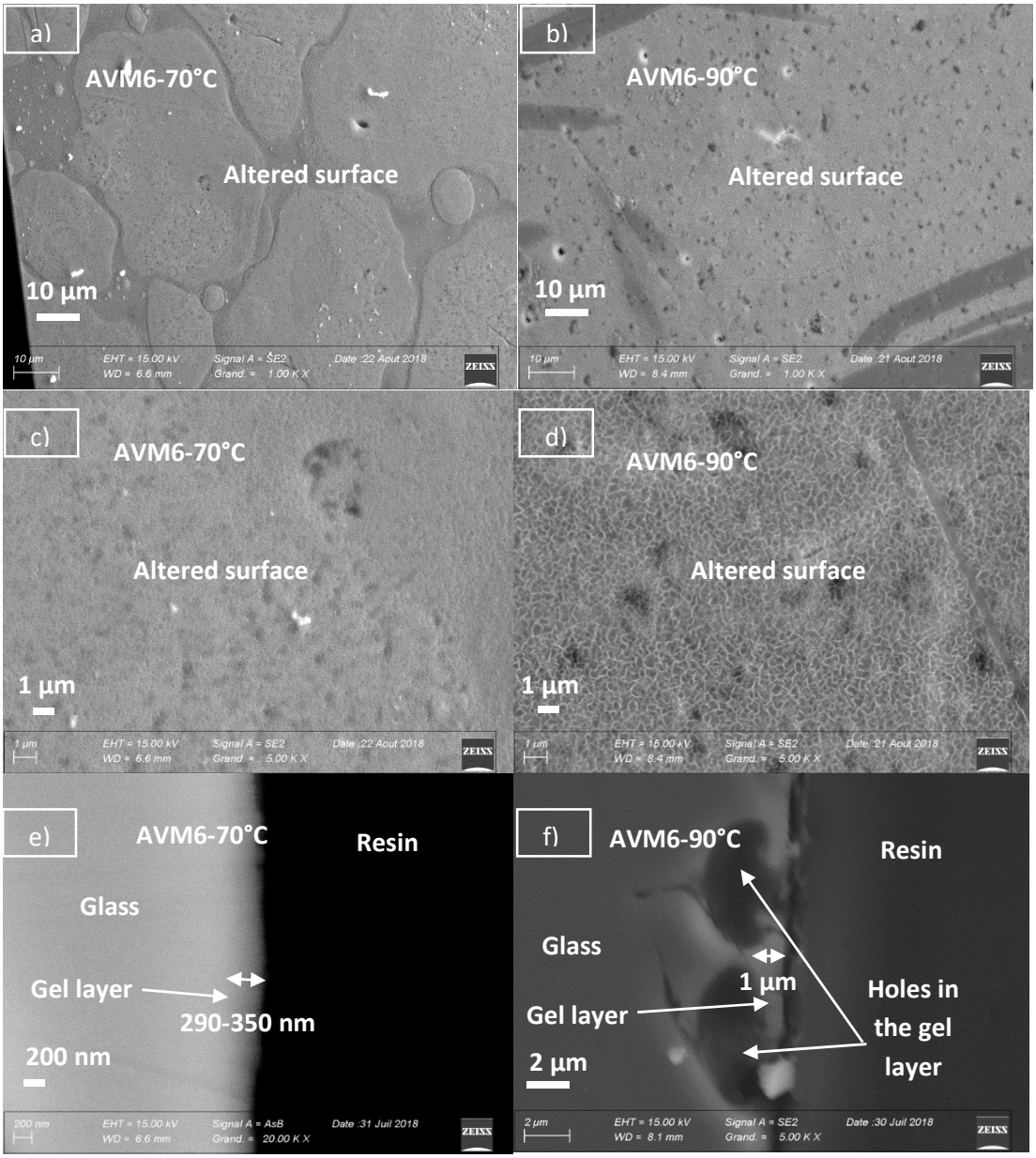

Figure 1 SEM images of AVM6 glass altered in vapor phase at 70°C (left- a, c, e) and 90°C (right- b, d, f) and 97% RH for 1 year. The top and middle images are direct observations of the altered surface while the bottom images show the cross-sections of the altered samples

Figure 2

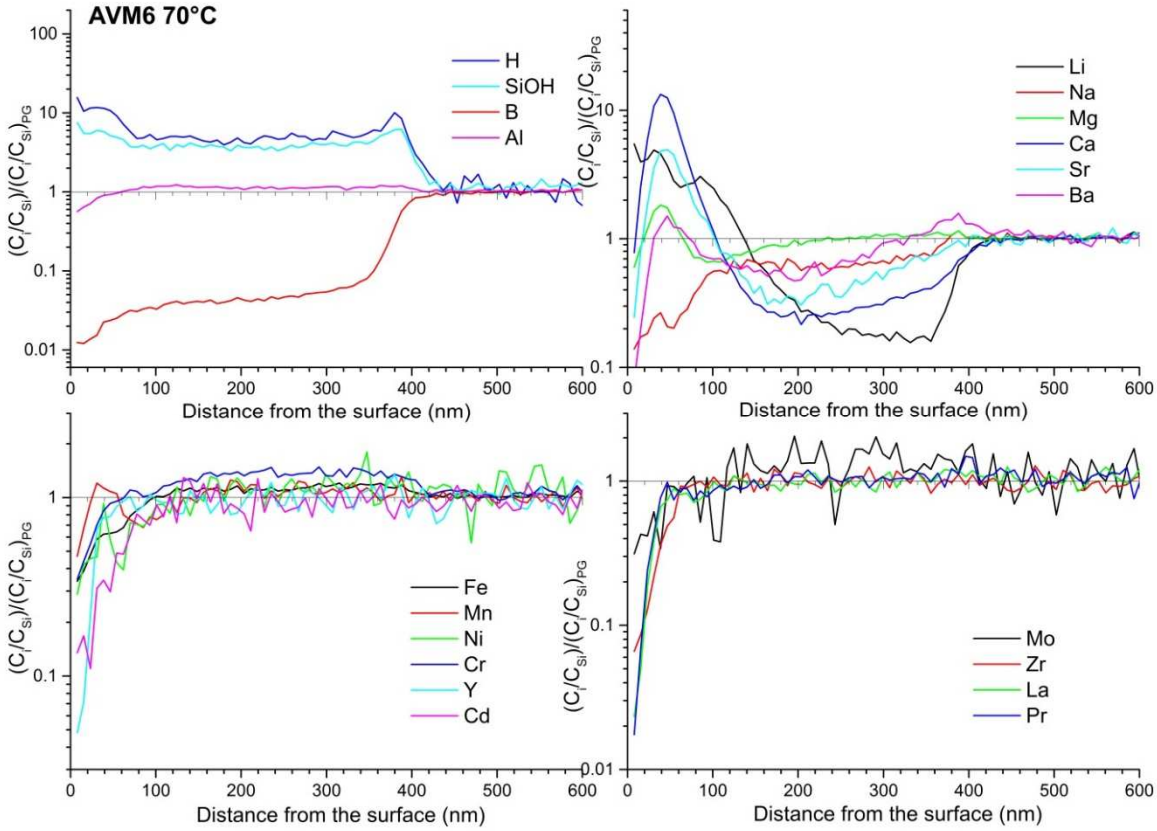

Figure 2 ToF-SIMS profiles (normalized with respect to the intensity of Si and pristine glass) for the glass AVM6 altered in vapor phase at 70°C and 97% RH for 1 year

Figure 3

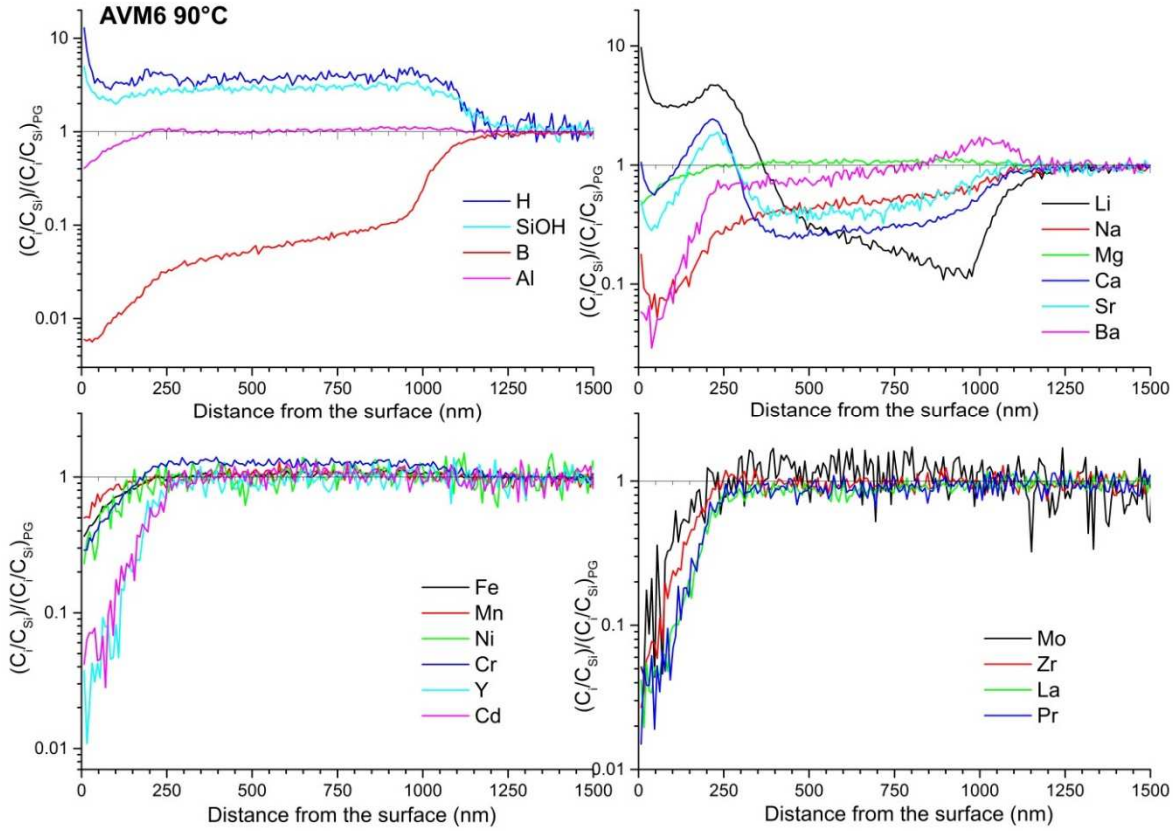

Figure 3 ToF-SIMS profiles (normalized with respect to the intensity of Si and pristine glass) for the glass AVM6 altered in vapor phase at 90°C and 97% RH for 1 year

Figure 4

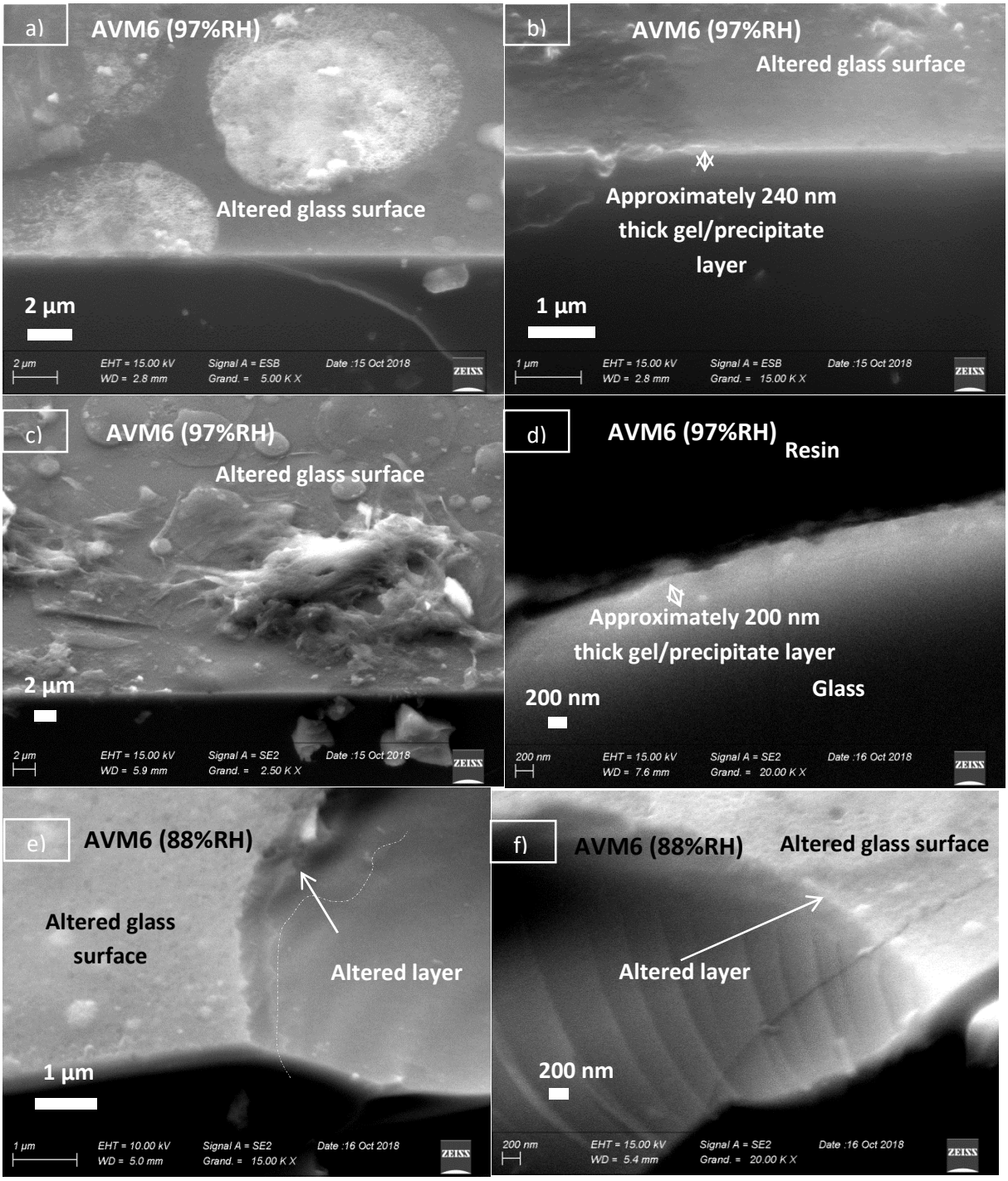

Figure 4 SEM images of AVM6 glass altered at 50°C and 97% RH (a, b, c and d) and 88% RH (e and f). The d image is a cross-section of the AVM6 sample altered at 97% RH. The remaining images are a direct observation of the altered sample

Figure 5

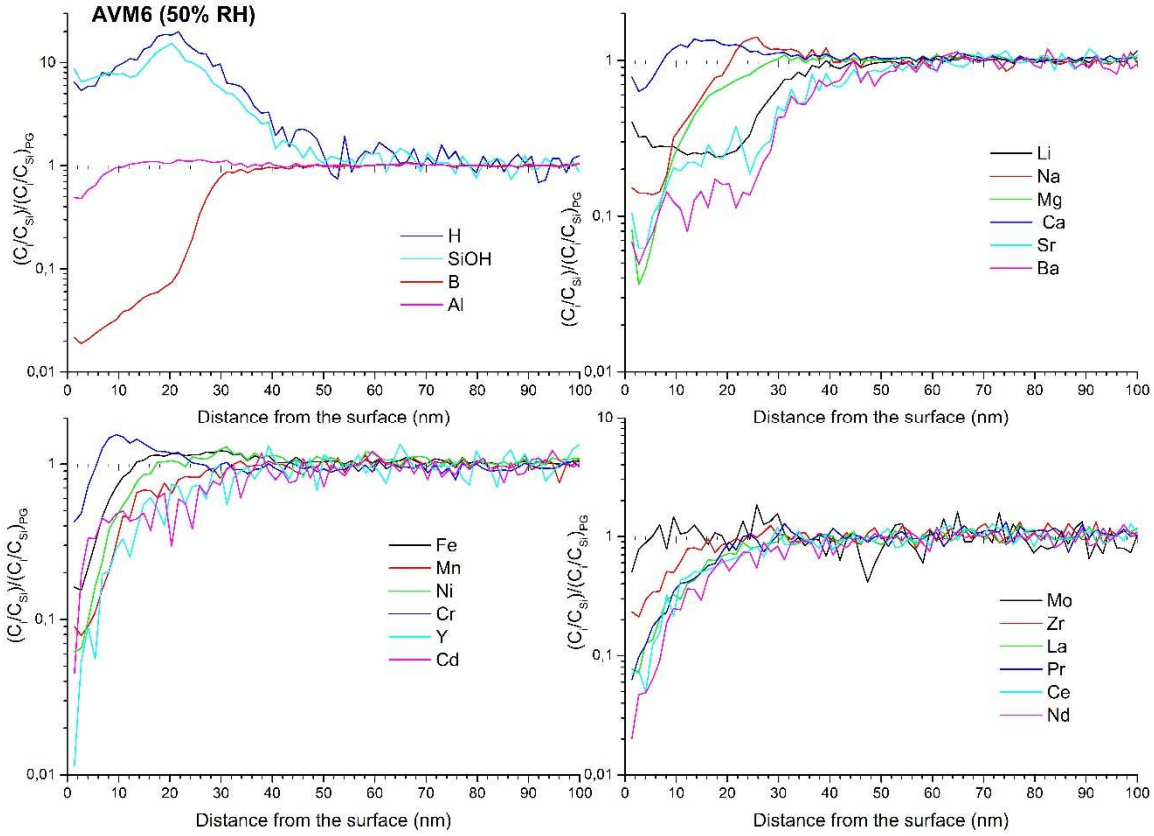

Figure 5 ToF-SIMS profiles (normalized with respect to the intensity of Si and pristine glass) for the glass AVM6 altered in vapor phase at 50°C and 50% RH for 1 year

Figure 6

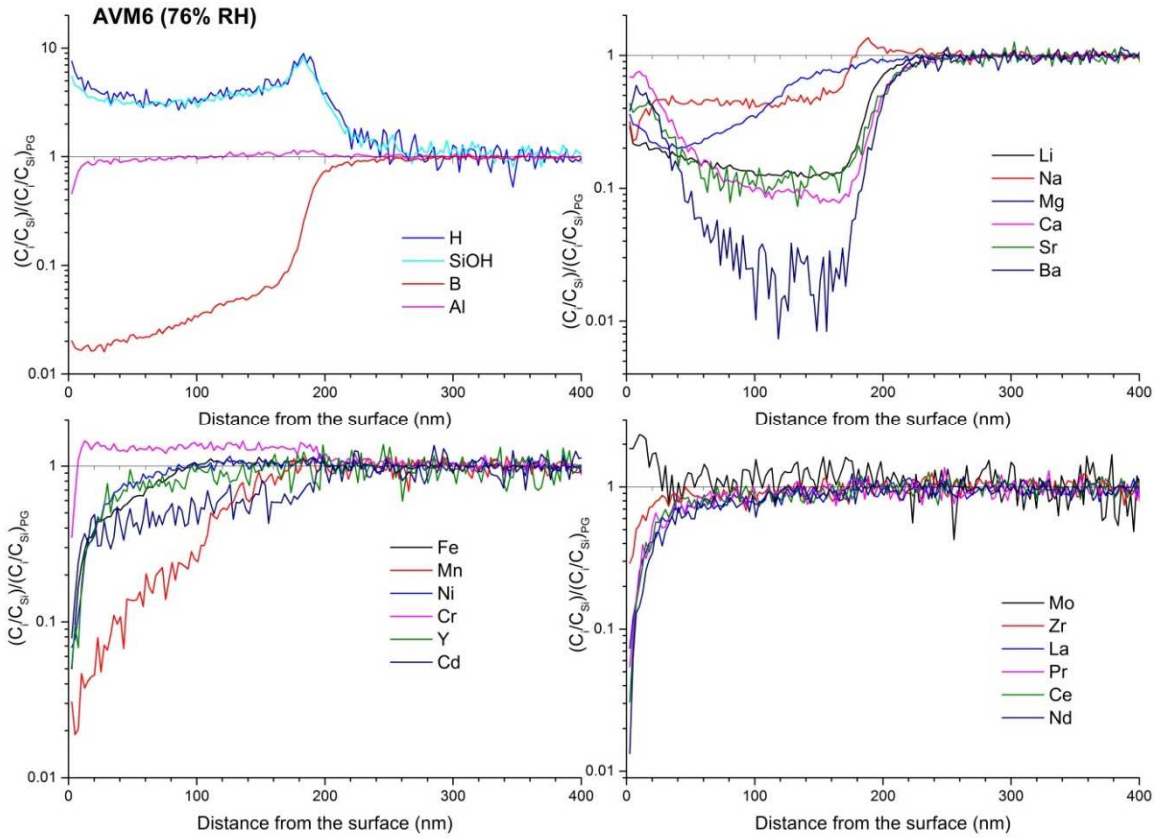

Figure 6 ToF-SIMS profiles (normalized with respect to the intensity of Si and pristine glass) for the glass AVM6 altered in vapor phase at 50°C and 76% RH for 1 year

Figure 7

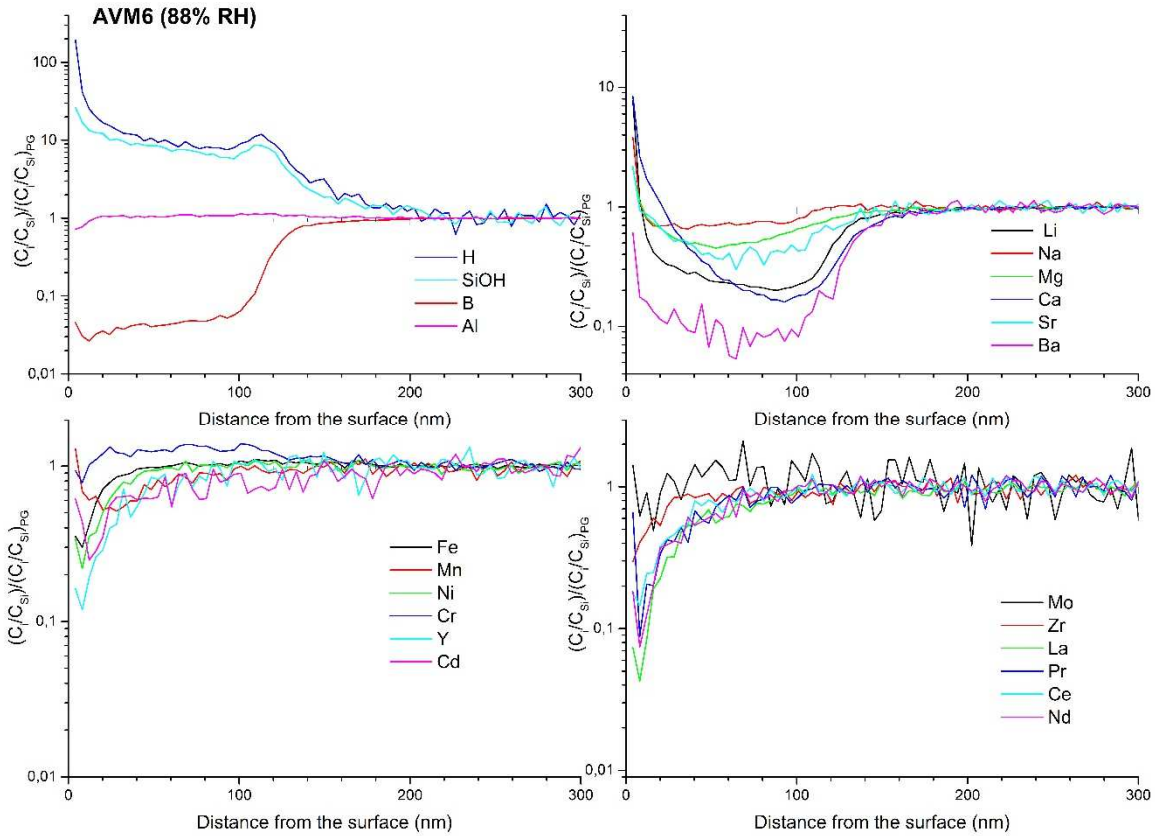

Figure 7 ToF-SIMS profiles (normalized with respect to the intensity of Si and pristine glass) for the glass AVM6 altered in vapor phase at 50°C and 88% RH for 1 year

Figure 8

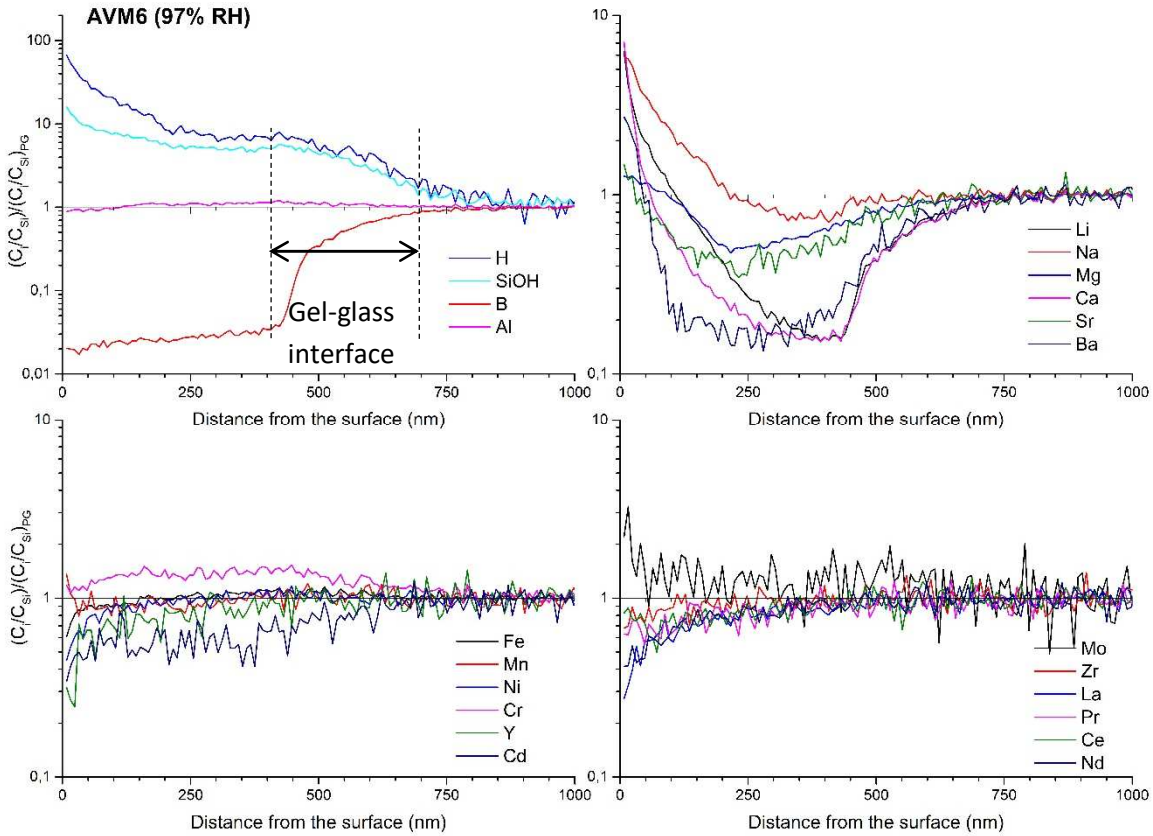

Figure 8 ToF-SIMS profiles (normalized with respect to the intensity of Si and pristine glass) for the glass AVM6 altered in vapor phase at 50°C and 97% RH for 1 year

Figure 9

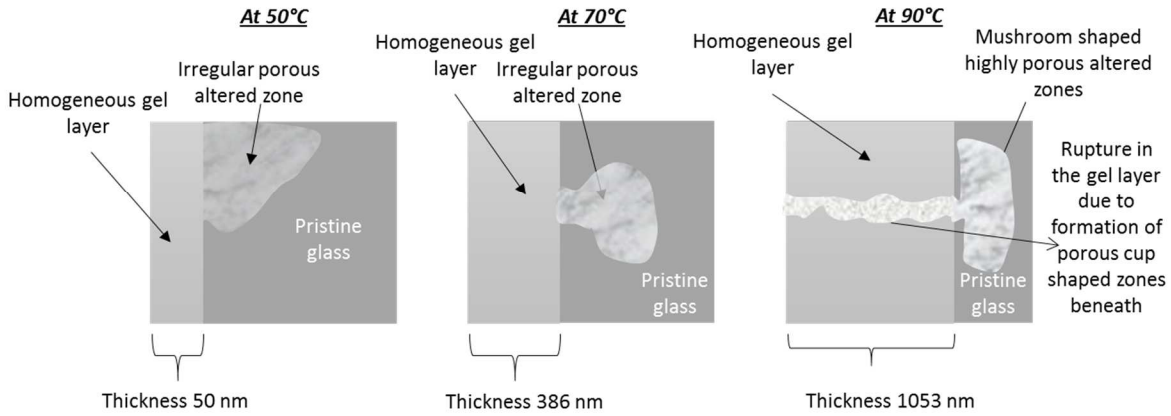

Figure 9 Schematic representation of the evolution of AVM6 glass altered layer morphology altered at different temperatures (95% RH at 50°C and 97% RH at 70°C and 90°C)

Figure 10

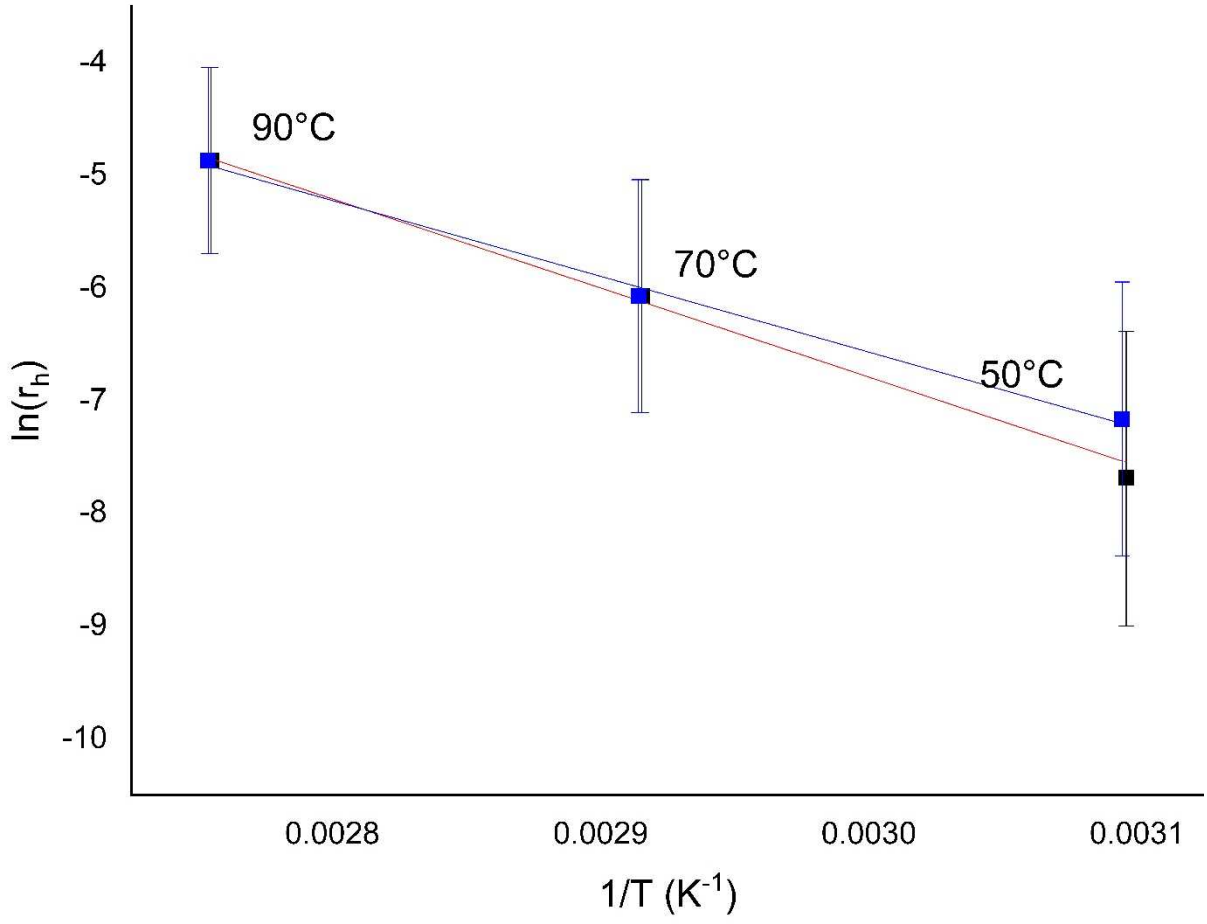

Figure 10 Plot of $\ln(r_h)$ vs $1/T$ (K^{-1}) for the AVM6 glass altered in vapor phase in the temperatures50°C (95%RH), 70°C (97%RH) and 90°C (97%RH); r_h represents the vapor hydration rate measured in g/m²day; The assignment of the blue line and the red line is described in section 4.1

11 Figure 11

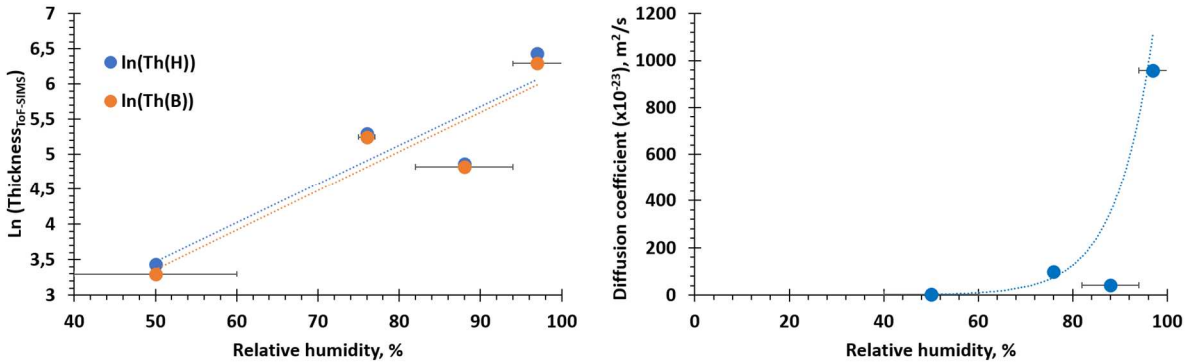

12

13 **Figure 11 (left) Evolution Natural logarithm of the thickness of hydrogen penetration and boron depletion depths**
14 **measured by ToF-SIMS with respect to RH; (right) Evolution of diffusion coefficient of hydrogen into the altered layer as a**
15 **function of the RH;**

16 Figure 12

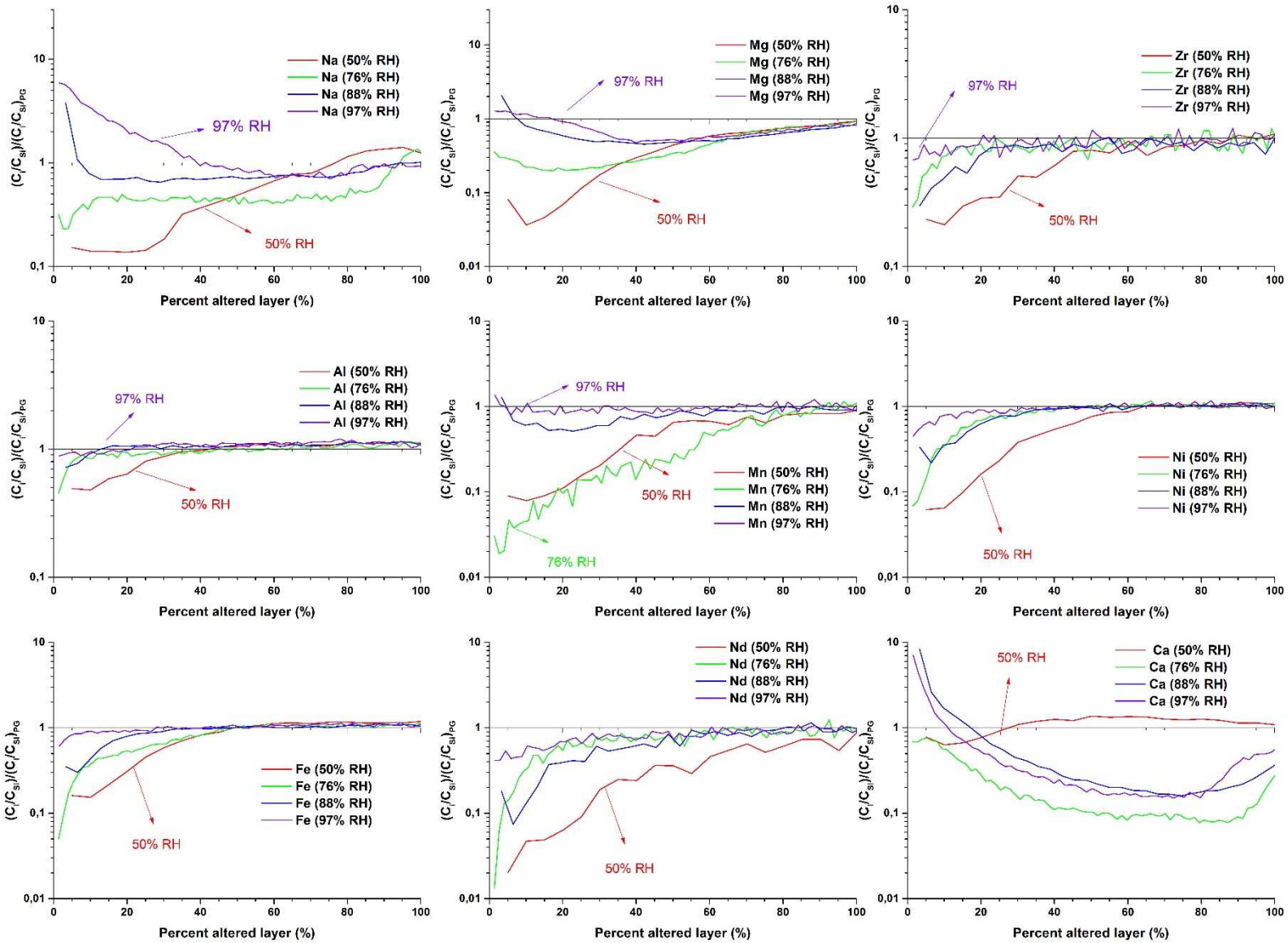
Na (50% RH)
Na (76% RH)
Na (88% RH)
Na (97% RH)
97% RH
50% RH
Mg (50% RH)
Mg (76% RH)
Mg (88% RH)
Mg (97% RH)
Zr (50% RH)
Zr (76% RH)
Zr (88% RH)
Zr (97% RH)
Al (50% RH)
Al (76% RH)
Al (88% RH)
Al (97% RH)
Mn (50% RH)
Mn (76% RH)
Mn (88% RH)
Mn (97% RH)
76% RH
Ni (50% RH)
Ni (76% RH)
Ni (88% RH)
Ni (97% RH)
Fe (50% RH)
Fe (76% RH)
Fe (88% RH)
Fe (97% RH)
Nd (50% RH)
Nd (76% RH)
Nd (88% RH)
Nd (97% RH)
Ca (50% RH)
Ca (76% RH)
Ca (88% RH)
Ca (97% RH)
Percent altered layer (%)
(C_i/C_Si)/(C_i/C_Si)_PG

18 **Figure 12 A comparison of the normalized ToF-SIMS profiles of Na, Mg, Zr, Al, Mn, Ni, Fe, Nd and Ca as a function of percent of altered layer for the AVM6 glass altered in vapor phase at**
19 **50°C and 4 RH values (100% corresponds to the altered layer depth (gel-pristine glass interface) calculated from B profiles)**